BOOK OF PROCEEDINGS
2019

25-29 OCTOBER 2019
Sakarya, TURKEY

SAKARYA UNIVERSITY

FACULTY OF ARTS AND SCIENCES

DEPARTMENT OF CHEMISTRY

5th INTERNATIONAL TURKIC WORLD CONFERENCE ON CHEMICAL SCIENCES AND TECHNOLOGIES

(ITWCCST 2019)

25-29 OCTOBER, 2019

SAKARYA

TURKEY

Chair of Conference

Prof. Dr. Abdil ÖZDEMİR

General Coordinator

Prof. Dr. Ahmet TUTAR

Congress Secretary

Semih BİTİM

Selim KAYA

Ömer Faruk TUTAR

Ramazan ERENLER

Raşit Fikret YILMAZ

Yavuz DERİN

Organizing Committee

M. Hakkı ALMA, Turkey

Abdolali ALEMİ, Iran

Atiqur RAHMAN, Bangladesh

Etibar ISMAILOV, Azerbaijan

Hacali NECEFOĞLU, Turkey

Rashid AHMAD, Pakistan

Hüseyin ALTUNDAĞ, Turkey

Moneer Hameed TOLEPHIH, Iraq

İmameddin AMİRARSLAN, Azerbaijan

Beytullah EREN, Turkey

Murat TUNA, Turkey

Ramazan ERENLER, Turkey

Kudret YILDIRIM, Turkey

Kemal KARADENİZ, Turkey

Gülnur ARABACI, Turkey

Esra ALTINTIĞ, Turkey

Mustafa Durmuş, Turkey

Ömer Faruk TUTAR, Turkey

Raşit Fikret Yılmaz, Turkey

Yadigar Adiloğlu, Turkey

Yavuz Derin, Turkey

Büşra Albayrak, Turkey

Akın Özdemir, Turkey

Zahidül Islam, Bangladesh

Gökçe Hilal Taşan, Turkey

Ayşenur Çetintaş, Turkey

Aslı Koç, Turkey

Scientific Committee

Abdil ÖZDEMİR	Sakarya University, Turkey
Abdolali ALEMİ	Tabriz State University, Iran
Ahmet TUTAR	Sakarya University, Turkey
Akhat MUSTAFIN	Bashkir State University, Russia
Akmal GABALLA	Zagazig University, Egypt
Alaa Abdul Hussein ABDUL RASOOL	Rector of Universty of Baghdad, Iraq
Alireza KHATAEE	Tabriz State University, Iran
Anton MEDEN	University of Ljubljana, Slovenia
Arye TISHBEE	Weizmann Institute of Science, Israel
Asiya MUSTAFINA	A.E. Arbuzov Institute of Organic and Physical Chemistry, Kazan, Republik of Tatarstan, Russia
Atiqur RAHMAN	Islamic University, Bangladesh
Dilgam TAGİYEV	Azerbaijan National Academy of Sciences, Azerbaijan
Erdoğan KÜÇÜKÖNER	Süleyman Demirel University, Turkey
Erdos ONGARBAEV	Al-Farabi Kazakh National University, Kazakhstan
Erol PEHLİVAN	Selçuk University, Turkey
Etibar ISMAILOV	Azerbaijan National Academy of Sciences, Azerbaijan
Hacali NECEFOĞLU	Kars Kafkas University, Turkey
Hakan YOĞURTÇU	Munzur University, Turkey
Hamada ABDELRAHMAN	Cairo University, Egypt
Igor KALININ	National Pedagogical Dragomanov University, Ukraina
Igor PLAZL	University of Ljubljana, Slovenia
İbrahim IŞILDAK	Yıldız Technical University, Turkey
İbrahim MAMEDOV	Baku State University, Azerbaijan
İsmail KIRAN	Eskişehir Osmangazi University, Turkey
Jamal MUSAEV	Emory University, USA

Yavuz ONGANER	Atatürk University, Turkey
Yunus Ali ÇENGEL	University of Nevada, USA
Victoria Anatolyivna TSYGANKOVA	The National Academy of Sciences, Ukraine
Zdeněk ČERNOŠEK	University of Pardubice, Czech Republic
Zekai ŞEN	İstanbul Technical University, Turkey
Zinfer ISMAGILOV	Institute of Coal Chemistry and Material Science, Russia

Dear Participants;

The 5th International Turkic World Conference on Chemical Sciences and Technologies organized by collaboration of Sakarya University Faculty of Arts and Science Chemistry Department. We are happy that the conference was held in such a beatiful city and wonderful country to which we have many historical relations.

Chemistry is a central science, because a basic knowledge chemistry is essential for healt, agriculture, engineering and natural sciences. The technological and scientific developments eliminate the sharp lines among the brances of science. Any new development in science will affect the whole science world and we believe that chemistry has a privilege among them. Thus, chemistry has broader applications and intersects with many other of them.

We are happy to see that the conference held last year in Sarajevo enabled many scientists to form good relationships that resulted in new projects. We wish that this conferance opens new doors to new projects and new relations as in last year. In this respect, we desired that the scienctists in Turkic world come here, meet and creat new projects together.

The scientist attended the conference was from 12 different country and mostly from Turkey, Iraq and Azerbaijan. Total 145 scientist, educater, industrialist and from other fields were registrated in the conference. The total number of submission were 123 and after a careful evaluation 134 submissions were accepted by our scientific committee and 61 of them were accepted as oral presentation and 66 of them were accepted as poster presentation and abstract part of all those presentation was taken place in the conference booklet.

We would like to thank to Rector of Sakarya University Prof. Dr. Fatih ŞAVAŞAN for giving us permission and also supporting us both financially and morally and also we thank to the Dean of Faculty of Arts and Science of Sakarya University Prof. Dr. Yılmaz DAŞÇIOĞLU. And the most importantly I would like to thank to all the participants individually who came from away to join this conference.

Prof. Dr. Abdil ÖZDEMİR
Chair of Conference

CONTEXT

ITWCCST 2019
5th International Turkic World Conference on Chemical Sciences and Technologies
25 - 29 October, Sakarya / Turkey
2019.itwccst.org

Further and Versatile Functionalization of Substituted Quinoline Analogues

Salih ÖKTEN*

Department of Mathematic and Science Education, Division of Science Education, Faculty of Education, Kırıkkale University, 71450, Yahşihan, Kırıkkale, Turkey

salihokten@kku.edu.tr

Keywords: Quinoline, Bromination, Cyanoquinoline, Methoxyquinoline

INTRODUCTION

The quinoline moiety forms the key skeleton of several natural and pharmacologically active compounds which display a broad spectrum of biological activities.[1-2] There has been tremendous interest in developing efficient methods for the synthesis of quinoline derivatives with significant applications in the fields of medicinal, bioorganic, industrial and synthetic organic chemistry.

Several methods for the synthesis of haloquinolines have been reported, including direct halogenation, which always suffers from poor regioselectivity and overhalogenation,[3] but only a few methods for the regioselective synthesis of 3-haloquinolines are known.[4] Due to the lack of availability of suitable procedures for the poly bromination/ functionalization of quinoline core. This area still remains unlaboured. We explored different and convenient approaches based on multifunctionalization of quinoline core itself. Actually our stragies are based on bromination of 1,2,3,4-tetrahydroquinoline and substitution of bromo quinolines/tetrahydroquinolines or their electrophichilic/nucleophilic substitions and Suzuki coupling reactions (Scheme 1).[5-6]

This study indicated that tetrahydroquinolines are very reactive towards bromine giving 3-brominated aromatic derivatives.

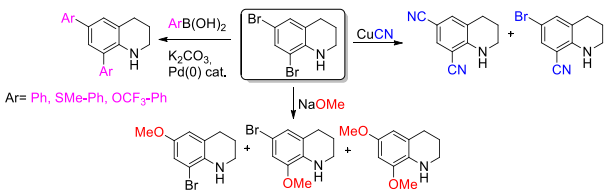

Scheme 1. Preperation of starting materials

RESULTS AND DISCUSSION

Previously prepared methoxy cyano and aryl substituted tetrahydroquinolines were further bromination to get polyfunctional quinoline derivatives.

First, treatment of 6-bromo-8-cyanotetrahdyroquinoline by molecular bromine was gave 3,6-dibromo-8-cyanoquinoline as a sole product. However, 6,8-dicyanotetrahydroquinoline interstingly dimerizeted during further bromination (Scheme 2).

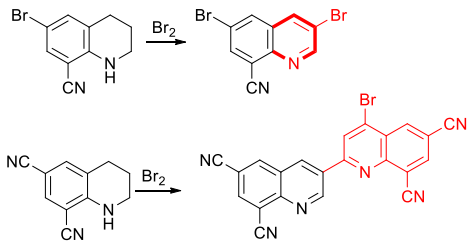

Scheme 2. Bromination of cyano tetrahydroquinolines

Bromination of 6-bromo-8-cyano-1,2,3,4-tetrahydroquinoline gave corresponding 3-brominated quinoline derivatives (Scheme 2).[5] This methodology uses neither metal catalyzed cyclizations nor acid catalyzed cycloadditions. The process constitutes a rapid and convenient method for obtaining selective brominated aromatic compounds as the sole products in high yields.

The study on bromination of tetrahydromethoxy quinolines with different equivalents of bromine was worked. The bromination of methoxy tetrahydroquinoline derivatives was gave mono, di, tri bromo methoxyquinoline derivatives. Bromination was occurred in both *N* cycle and benzene ring of tetrahydroquinoline (Scheme 3). While bromination of 6-bromo-8-methoxytetrahydroquinoline with three equivalents of bromine afforded 3,6-dibromo-8-

methoxyquinoline, bromination with four equivalents of bromine gave 3,5,6-tribromide (Scheme 3).

6,8-Dimethoxytetrahydroquinoline was brominated with 3 equivalents of bromine and the monobromide was obtained as the sole product in high yield in reaction conditions similar to those of of 6-bromo-8-methoxytetrahydroquinoline. On the other hand, bromination of 6,8-Dimethoxytetrahydroquinoline with four equivalents of bromine gave 3,5-dibromide in high yield (Scheme 3).

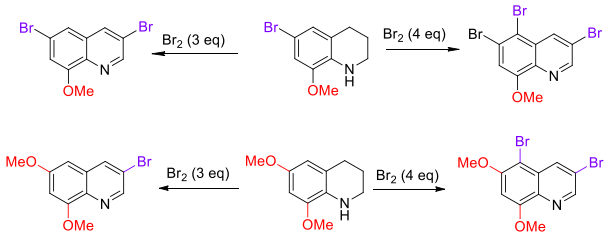

Scheme 3. Bromination of methoxy tetrahydroquinolines

CONCLUSION

Two regioselective routes are described for the convenient preparation of 3- and 5-brominated methoxy quinolines. Quinoline cores are selectively functionalized at both the C-3 and C-5 positions under mild reaction conditions.

We found that methoxy 1,2,3,4-tetrahydroquinolines firstly were brominated at the C-3 and C-5 positions to give corresponding bromoquinolines.

ACKNOWLEDGEMENTS

This study was supported by TÜBİTAK (Grand No: 112T394)

REFERENCES

[1]Muscia, G. C.; Bollini, M.; Carnevale, J. P.; Bruno, A. M.; Asis, S. E. *Tetrahedron Lett*. **2006,** 47, 8811-8815.
[2]Solomon, V. R.; Lee, H. *Eur. J. Pharmacol.* **2009**, 625, 220-233.
[3]Kumar L, Mahajan T, Agarwal DD. Green Chem. 2011,13, 2187-2196.
[4]Tummatorn J, Poonsilp P, Nimnual P, Janprasit J, Thongsornkleeb C, Ruchirawat S. J Org Chem. 2015, 80, 4516.
[5]Ökten, S.; Çakmak, O. Tetrahedron Lett. **2015**, 56, 5337-5340.
[6]Çakmak, O.; Ökten, S. Tetrahedron. **2017**, 73, 5389-5396.

ITWCCST 2019
5th International Turkic World Conference on Chemical Sciences and Technologies
25 - 29 October, Sakarya / Turkey
2019.itwccst.org

Investigation of Carbonic Anhydrase Inhibitory Profiles of Cyanoquinolines

Salih ÖKTEN[1,*], Ümit Muhammet KOÇYİĞİT[2]

[1]*Department of Mathematic and Science Education, Division of Science Education, Faculty of Education, Kırıkkale University, 71450, Yahşihan, Kırıkkale, Turkey*

[2]*Department of Medical Techniques, Vocational School of Health Services, Cumhuriyet University, 58140, Sivas, TURKEY*

salihokten@kku.edu.tr

Keywords: Cyanoquinolines, Carbonic anhydrase, Inhibition

INTRODUCTION

Quinoline scafold forms a highly attractive ring system in organic chemistry, pharmacologically active compounds due to having wide range of biological activities.[1-2] The substituted quinolines displays high anti-pesticide against *nematode* and *Haemonchus contortus*,[3] agricultural predatory, significant antibacterial activity,[4] anti-inflammatory, analgesic, antipyretic activities and efficient inhibition of the COX-2 enzyme.[5] However, the there are resricted articles on carbonic anhydrase inhibitory activities of quinoline derivatives. Notably, cyano quinoline compounds substituted at the C-3 position can act to deactivate the action of growth factor receptor protein tyrosine kinases.[6–8] Agents with cyano groups also act as small molecule inhibitors, binding with biological systems.[9] A significant body of work has been reported on the synthesis and derivatization of the quinoline substructure.

Carbonic anhydrase (CA) is an important enzyme containing metal in the active site. It catalyzes the reversible hydration of carbon dioxide (CO_2) to proton (H^+) and bicarbonate (HCO^{-3}).[10] The ability of some bivalent metal ions such as Fe^{2+}, Cd^{2+} and Hg^{2+} has been shown to easily bind to the three-histidine residue within the CA active site in transmetallation experiments.[11]

In this study, we have explored the inhibition potentials of substituted quinoline derivatives against two physiologically relevant cytosolic CA isoforms, hCA I and hCA II using esterase assay method. Acetazolamide (AZA) was used as a standard drug. CA I and II isoforms inhibition data of compounds are summarized and their IC_{50} values expressed as nanomolar (nM).

RESULTS AND DISCUSSION

In our previous publications,[12-13] the copper induced cyanation of 6,8-dibromoquinoline was investigated and and 6,8-dibromo-1,2,3,4-tetrahydroquinoline. 6,8-Dibromoquinoline was reacted with CuCN in refluxing DMF to afford a mixture of mono- and dicyanoquinolines (Scheme 3). The effect of reaction duration on the product ratio was investigated.

When 6,8-dibromo-1,2,3,4-tetrahydroquinoline 2 was treated with CuCN in refluxing DMF, the ^{1}H NMR spectrum indicated formation of a mixture of mono and dicyano tetrahydroquinolines which varied in composition by reaction time. It was observed that after 4 h, two cyano tetrahydroquinoline derivatives had formed as assigned by ^{1}H NMR spectroscopy.

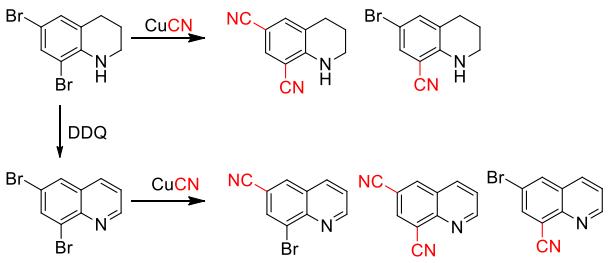

Scheme 1. Cyanization of bromo tetrahydroquinolines and quinolones

Table 1. IC_{50} values of cyanoquinoline derivatives against hCA I and hCA II

	IC_{50} (nM)		K_i (nM)	
	hCA I	hCA II	hCA I	hCA II
	281.52	33.84	306.82±8.04	335.96±42.07
	305.04	39.01	294.62±1.74	304.75±65.66
	**39.52**	**52.84**	**46.04±8.63**	**54.95±5.93**
	100.80	83.93	926.33±8.64	963.33±95.35
	**83.04**	**10 5.94**	**103.64±2 0.63**	**119.05±13 .94**
	507.27	49.26	635.33±7.26	684.03±88.31
	406.92	40.75	444.28±6.84	417.04±73.80
AZA	110.70	11 88.01	1005.47± 75.60	1104.43±9 5.55

The all of the substituted quinoline analogs were remarkably inhibited the slow cytosolic isoform hCA I, taking part in important physiological and pathological processes in many tissues and organs), with K_is ranging between 46.04 and 926.33 nM. 6,8-Dicyanotetrahydroquinoline was determined as the best inhibitors for this isoform with K_i values of 46.04 nM (Table 1). Moreover, 5-aceta-imido-1,3,4-thiadiazole-2-sulfonamide (AZA), broad-specificity CA inhibitor and used for the treatment of altitude sickness, cystinuria, idiopathic intracranial hypertension, glaucoma, epileptic seizure, was recorded Ki value of 1005.47±75.60 nM against hCA I. The high concentration of the hCA II led to several diseases such as glaucoma, osteoporosis and renal tubular acidosis (Ökten et al., 2019a). The cytosolic isoenzyme hCA II, substituted quinoline had Ki values ranging from 54.95 to 963.33 nM. The inhibitory potentials of substituted quinoline derivatives against the hCA II had similar behaviour to that against hCA I. In addition, AZA had a medium inhibition potencial against this isoform with a Ki value of 1104.43 nM.

CONCLUSION

Both recently synthesized substituted quinoline bearing cyano groups were tested for their antibacterial, anticancer activities *in vitro* and enzyme inhibition effects. We have shown that substituted quinolines have significant potential as being enzyme inhibitor against hCA I and hCA II. Also, all of the substituted quinolines effectively reduced enzyme activities of hCA I, and hCA II at the nanomolar concentrations. The substituted quinoline analogues can be drug candidate of the CAIs, for therapy of some diseases such as epilepsy, osteoporosis, glaucoma, gastric and duodenal ulcers, neurological disturbances.

ACKNOWLEDGEMENTS

This study was supported by TÜBİTAK (Grand No: 112T394).

REFERENCES

[1]Nandhakumar, T.; Suresh, A. L.; Judge, C.; Kannan, V. R.; Mohan P. S. *Eur J Med Chem* **2007**, 42, 1128.
[2]El Shehry, M. F.; Ghorab, M. M.; Abbas, S. Y.; Fayed, E. A.; Shedid, S. A.; Ammar, Y. A. *Eur J Med Chem* **2018**, 143, 1463.
[3]Huang, C. Q.; Wilcoxen, K.; McCarthy, J. R.; Haddach, M.; Webb T.R.; Gu, J.; Xie, Y.F.; Grigoriadis, D. E.; Chen, C. *Bioorg Med Chem Lett* **2003**, 13: 3375.
[4]Wang, X.; Xie, X.; Cai, Y.; Yang, X.; Li, J.; Li, Y.; Chen, W.; He, M. *Molecules* **2016**, 21, 340.
[5]Manikandan, A.; Ravichandran, S.; Sathiyanarayanan, K. I.; Sivakumar, A.; *Inflammopharmacol* **2017**, 25, 621.
[6]Berger, D. M.; Dutia, M.; Powell, D.; Floyd, M. B.; Torres, N.; Mallon, R.; Wojciechowicz, D.; Kim, S.; Feldberg, L.; Collins, K.; Chaudhary, I. *Bioorg. Med. Chem*. **2008**, 16, 9202.
[7]Wissner, A.; Johnson, B. D.; Reich, M. F.; Floyd Jr.; M. B.; Kitchen, D. B.; Tsou H. R. Substituted 3-Cyano Quinolines. US Patent 6,002,008, **1999**.
[8]Zhang, N.; Wu, B.; Eudy, N.; Wang, Y.; Ye, F.; Powell, D.; Wissner, A.; Feldberg, L. R.; Kim, S. C.; Mallon, R.; Kovacs, E. D.; Toral-Barza, L.; Kohler, C. A. *Bioorg. Med. Chem. Lett*. **2001**, 11, 1407.
Fleming, F. F.; Yao, L.; Ravikumar, P. C.; Funk, L.; Shook, B. C. J. Med Chem. 2010, 53, 7902.
[10]C. Yamali, H. I. Gül, A. Ece, P. Taslimi, I. Gülçin, Chem. Biol. Drug Des. 91 **2018**, 854-866.
[11]P. Taslimi, I. Gülçin, B. Ozgeris, S. Goksu, F. Tümer, J. Enzym. Inhib. Med. Chem. 31, **2016**, 152-157.
[12]Ökten, S.; Çakmak, O.; Erenler, R.; Tekin, Ş.; Yüce, Ö. Turk. J. Chem. 2013, 37, 896.
[13]Ökten, S.; Çakmak, O. Tetrahedron Lett. **2015**, 56, 5337-5340.

ITWCCST 2019
5th International Turkic World Conference on Chemical Sciences and Technologies
25 - 29 October, Sakarya / Turkey
2019.itwccst.org

Biological Evaluation of Brominated Indenoquinolines as Anticancer Agents

Salih ÖKTEN[1,*], Ali AYDIN[2], Ahmet TUTAR[3]

[1]*Department of Mathematic and Science Education, Division of Science Education, Faculty of Education, Kırıkkale University, 71450, Yahşihan, Kırıkkale, Turkey*

[2]*Tuzla State Hospital, Biochemistry Labratory, İçmeler District, Piri Reis Street, No:74, 34947, Tuzla, İstanbul, Turkey*

[3]*Department of Chemistry, Faculty of Art and Science, Sakarya University, 54100, Serdivan, Sakarya, TURKEY*

salihokten@kku.edu.tr

Keywords: Indenoquinolines, Anticancer activity, Inhibition

INTRODUCTION

Indenoquinolines contain quinoline scafolds bearing tetra aromatic heterocycle and considered as important chemical and biological agents due to their variable biological activities such as 5-HT-receptor binding and anti-inflammatory.[1] They have also showed antitumor agents,[2] antimalarials,[3] and also AChEIs.[4] Thus, the synthesis of indenoquinolines has attracted considerable attention. However, there are restricted reports about synthesis of substituted indenoquinoline amine, displayed AChE inhibitory activity. Some reported studies showed that halogenated indenoquinoline analogues have better inhibitory activity compared with unsubstituted ones.[5] This study reported that especially fluoro substituted at C-2 position of benzene ring fused 1-H indene having more AChE inhibitory activity potential compared with methoxy, chloro-substituted indenoquinoline amine derivatives.[5]

This study presents the antiproliferative activities of mono bromo indenoquinolines against HeLa (cervical cancer cell line) and HT29 (colon cancer cell line).

RESULTS AND DISCUSSION

In our previous papers,[6] one-pot synthesis was described for functional bromo tetracyclic indenoquinoline amine derivatives were obtained because heterocyclic aromatics are key structures in a large amount of pharmacological compounds.[7-8] Due to that the direct bromination leads to some problems in obtaining brominated *N* function aromatics.[9] We attempted Friedlander reactions between 2-aminobenzonitrile or corresponding brominated 2-aminobenzonitriles and bromoindan-1-ones, instead of direct bromination of indenoquinoline nucleus.

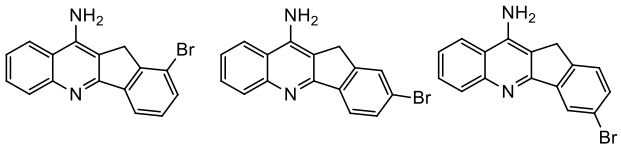

Figure 1. Mono bromo indenoquinolineamines

Many anticancer drug candidates have been withdrawn from market due to their serious side effects, loss of sensitivity to drugs, and limited use for many cancer types. In the present study, the monobromo indenoquinoline derivatives (Figure 1) were prepared according to reported procedure by our research group[9] and investigated for their anticancer and cytotoxicities against HeLa and HT29 cell lines according to the MTT protocol. The half-maximal inhibitory concentration (IC_{50}) of these molecules were calculated using Four-Parameter Logistic Function, as well.

The tested compounds caused selective antitumor properties against all tested cell lines (Table 1). All compound**s** depicted significant antiproliferative effect (IC_{50} values 19-37 µg/mL) against HeLa cancer cell lines (Table 1). In HT29 cell lines, compound **1** (IC_{50} value 11 µg/mL) and **2** (IC_{50} value 28 µg/mL) showed a potent antitumor effect (Table 1). When the IC_{50} values of all the above-mentioned compounds are considered, effective ones have better antiproliferative effects compared to the positive control group, 5-FU (Table 1).

Table 1. IC_{50} values of bromo indenoquinoline aminederivatives against HeLa and HT29 cell lines

Compounds ($\mu g/mL$)	HeLa IC_{50}	HT29 IC_{50}
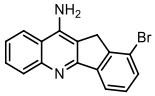	19	11
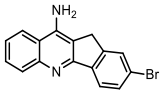	31.5	262.7
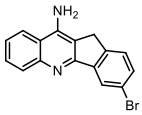	37	28
5-FU	65.6	68.2

CONCLUSION

The most of tested compounds exhibit much more potent antiproliferative activity than positive controls against the cancer cells (IC_{50} values 19 – 37 µg/mL). In consequence, mono bromo indenoquinolines can be anticancer agent candidate against HeLa and HT29 cancer cell lines.

ACKNOWLEDGEMENTS

This study was supported by SAÜ BAP (Grand No: Project number: 2014-02-04-008).

REFERENCES

[1]Anzini, M.; Cappelli, A.; Vomero, S.; Cagnotto, A.; Skorupska, M. *Med. Chem. Res.* **1993**, 3, 249.
[2]Deady, L. W.; Desneves, J.; Kaye, A. J.; Finlay, G. J.; Baguley, B. C.; Denny, W. A. *Bioorg. Med. Chem.* **2000**, 8, 977.
[3]Venugopalan, B.; Bapat, C. P.; Desouza, E. P.; Desouza, N. J. *Indian J. Chem. B* **1992**, 31, 35.
[4]Standridge, J. B. *Clin. Ther.* **2004**, 26, 615.
[5]Rampa, A. Bisi, A. Belluti, F. Gobbi, S. Valenti, P. Andrisano, V. Cavrini, V. Cavalli, A. Recanatini, M., *Bioorg. Med. Chem.* **2000**, 8, 497.
[6]Ekiz, M., Tutar, A., **Ökten**, **S.,** Bütün, B., Koçyiğit, Ü. M., Taslimi, P., Topçu, G., Archiv der Pharmazie, **2018,** 351, 9, e1800167.
[7]Ökten, S., Çakmak, O., Tekin, Ş., *Turk. J. Clin. Lab.* **2017**, 8, 152.
[8]Ökten, S., Çakmak, O., Tekin, Ş., Köprülü, T.K., *Lett. Drug Des. Dis.* **2017**, 14, 1415.
[9]Ökten, S., Çakmak, O., *Tetrahedron Lett.* **2015**, 56, 5337.

ITWCCST 2019
5th International Turkic World Conference on Chemical Sciences and Technologies
25 - 29 October, Sakarya / Turkey
2019.itwccst.org

Molecular Docking Studies of Some Pyridazinone Derivatives with Anticancer Effects

Mehmet Abdullah ALAGÖZ

[1]*Department of Pharmaceutical Chemistry, İnönü University Faculty of Pharmacy, Malatya, Turkey*

mehmet.alagoz@inonu.edu.tr

Keywords: Pyridazinone, Anticancer, SHSY5, Docking

INTRODUCTION

Cancer which could be defined as abnormal cell differentiation as the result of wrong DNA replication, is a disease that is hard to treat, widely endemic, highly mortal and increasing day by day, is characterized by abnormal somatic cell proliferation and quick expansion in the body. Cisplatin which is a compound which is used widely endemic for cancer treatment, has several side effects like nephrotoxicity, hepatotoxicity and reproductive toxicity and it was determined that because of these side effects usage of this compound is limited. Therefore, less toxic and safe drugs are produced compared to cisplatin, doing a lot of research related to the synthesis of novel chemotherapeutic agents and their treatment[1-3].

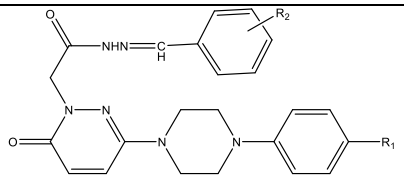

Comp.	R_1	R_2	Molecular Formula
1	-H	2-OCH_3	$C_{24}H_{26}N_6O_3$
2	-H	3-OCH_3	$C_{24}H_{26}N_6O_3$
3	-H	4-$N(CH_3)_2$	$C_{25}H_{29}N_7O_2$
4	-Cl	3-CH_3	$C_{24}H_{25}ClN_6O_2$
5	-Cl	3,5-diOCH_3	$C_{25}H_{27}ClN_6O_4$

Figure 1. Structure of compounds 1-5

3(*2H*)-Pyridazinone ring is a six-membered lactam ring system with $C_4H_4N_2O$ closed formula. It is known that the tautomeric balance is due to the presence of free hydrogen in the nitrogen atom in the 3(*2H*)-pyridazinone derivatives having no substituent at second position. Substituent-bearing derivatives of the pyridazinone ring, which is known to be aromatic in the ring nitrogen atom are weakly acidic and they form salts with strong bases or with ammonia and amines[4,5]. In recent years, many pharmacological activity studies have been carried out in compounds bearing the 3(*2H*)-pyridazinone structure, and studies have shown that these compounds have analgesic, antiinflammatory, antipyretic, antihypertensive, antiulcer, antioxidant, antiallergic, bronchospasmolytic, antibacterial, antifungal, antihelmmentic effect[6,9]. There are also compounds which were reported to have anticancer activity in the 3(*2H*)-pyridazinone structure[10-12]. In the litterateur a lot of synthesis which the basis structure of 3(*2H*)-pyridazinone has different functional group in side chains. It has also been reported that pyridazinones carrying substituents at fourth, fifth and sixth positions and containing phenyl groups attached to the ring nitrogen have cytostatic activity[11,12]. These results suggest that pyridazinone compounds may be useful in cancer chemotherapy, depending on the type of cancer, and that derivatives bearing different substituents may exhibit varying degrees of cytotoxic effect.

Because of these results related compounds were considered to be effective and safe for human health in order to treat cancer. In this context synthesized 3(*2H*)-phyridazinone derivative compounds that are proven to be an anticancer effect on cancer cell lines which is widely endemic compared to other cancers in the world and their efficiency on human health comparison with current chemotherapy drugs was determined.

Molecular modeling studies of active pyridazinone derivatives were carried out to investigate the structural activity.

RESULTS AND DISCUSSION

The activities of the compounds were evaluated in SH-SY5Y cell lines and the results are given in Table 1 as IC_{50}. Çiftçi at al. have stated that the compounds are may potential new drugs for cancer treatment[11].

Table 1. IC_{50} concentration of prydazinone compounds 1-5 (μM)

Comp.	SH-SY5Y
1	55,4
2	93,0
3	50,0
4	23,2
5	177,7

Fibroblast growth factor 1 (FGF1) is one of the most important factors in the development and differentiation of the central nervous system. Raguenez et al. reported a link between endogenous FGF1 signaling pathway and Bcl-2 in modulation of neuronal survival[13]. Therefore, this study was modeled with Bcl-2 protein.

Based on these results, molecular modeling studies of the compounds have been made.The three-dimensional models of the compounds were constituted using Maestro program (Schrödinger, LLC, NY) with the aid of MacroModel (Schrödinger, LLC, NY) software and the OPLS_2005 force field parameters, and were optimized by conjugated gradient method[14]. The ligand models were then ligated with LigPrep (Schrödinger, LLC, NY) software to determine the appropriate tautomeric and ionization states. The crystal structures Bcl-2 proteins retrieved from the RCSB Protein Data Bank (www.rcsb.org) by using the protein preparation wizard of Maestro for Bcl-2 4AQ3, 4IEH and 60OK PDB proteins[15]. Within this context, undesirable solvent molecules, ligands and segments in the crystal structures were deleted using Prime (Schrödinger, LLC, NY), Impact (Schrödinger, LLC, NY), Epic(Schrödinger, LLC, NY) and Propka softwares. molecular modeling studies are given in Table II.

Table 2. Molecular docking scores of 1-5

Comp.	4AQ3	4IEH	6O0K
1	-5.862	-6.887	-6.466
2	-6.147	-6.212	-5.845
3	-4.938	-6.858	-6.495
4	-5.197	-6.838	-7.243
5	-5.504	-6.626	-6.529

In particular, in the modeling studies, it was found that the activity results were compatible with 6O0K, a crystal structure of Bcl-2.

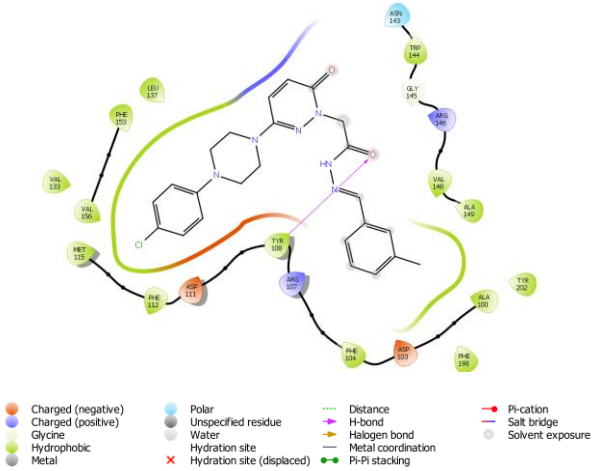

Figure 1. Interaction of compound **4** with the active site of the enzyme (6O0K)

Compound 4 was found to H bind with TYR108 in the active site of the enzyme. And also involved in the hydrophobic interaction with LEU137, PHE153, VAL156 MET115, PHE112, PHE104, ALA100, VAL148 and ALA149 in the active site of the enzyme.

In silico screening test was performed to determine ADME properties of compounds. Various parameters such as Total polar surface area (TPSA), molecular volume (MV), miLog P, number of rotatable bonds, number of hydrogen donor and acceptor atoms and aqueous solubility were calculated on the basis of Lipinski's rule of five which are closely related to the activity and drug properties of the compounds of this screening test have been calculated theoretically.

Table 3. Some pharmacokinetic parameters important for activity

	1	2	3	4	5
milogP	3.04	3.06	3.14	4.13	3.75
TSPA	92.07	92.07	86.08	82.83	101.30
MW	446.51	446.51	459.56	464.96	510.98
nON	9	9	9	8	10
nOHNH	1	1	1	1	1
nviolations	0	0	0	0	1
nrotb	7	7	7	6	8
volume	405.98	405.98	426.35	410.53	445.06
enzyme inhibitors	0.36	-0,35	0.29	0.38	0.34
Lipinski of five	0	0	0	0	1

When the results were examined, it was found that the TPSA value of the compound **5** with the lowest activity was higher than the others and MW value was more than 500. The most active compound **4** were found

to have the lowest TPSA value.

CONCLUSION

When the activities of the compounds were compared with the physicochemical parameters calculated by computerized methods, some parameters were found to be directly related to the activity (TPSA,MW).

This study supports that the researchers may use to calculate various physicochemical properties and to make molecular modeling studies before working with pyridazinone derivates.

REFERENCES

1. Institute, National Cancer. Defining Cancer: Cancer Fact sheet N°297". World Health Organization. http://www.who.int/mediacentre/factsheets/fs297/en/ (Accessed June 10, **2014**).
2. Institute, National Cancer. Targeted Cancer Therapies. http://www.cancer.gov/cancertopics/factsheet/Therapy/targeted (Accessed **2008**).
3. Islam, A.; Rodrigues, B.L.; Marzano, I.M.; Perreira-Maia, E.C.; Dittz, D.; Paz-Lopes, M.T.; Ishfaq, M.; Frézard, F.; Demicheli, C. *Eur. J. Med.Chem.*,**2016**, 109, 254-267.
4. Coad, P,; Coad RA; Clough S; Hyepock J, Salisbury, R,; Wilkins, C. J Org Chem **1963**,28(1),218–221.
5. Lamberth, C. Pest Manag Sci. **2013**,69,1106–1114.
6. Abd El-Ghaffar, N.F.; Mohamed, M.K.; Kadah, M.S.; Radwan, M.; Said, G.H.; Abd El-Al, S.N. *J. Chem. Pharm. Res.*, **2011**, *3(3)*, 248-259.
7. Malinka, W.; Kaczmarz, M.; Redzicka, A. *Acta Pol. Pharm. Dec*., **2014**, *61*,100-102.
8. Utku, S.; Gökçe, M.; Aslan, G.; Bayram, G.; Ülger, M.; Emekdaş, G.; Şahin, M.F.*Turk. J. Chem.*, **2011**, *35*, 331-339.
9. Şahin, M.F.; Badıçoğlu, B.; Gökçe, M.; Küpeli, E.; Yesilada, E. *Arch. Pharm. Pharm. Med*., **2004**, *33*, 445-452.
10. Özçelik, AB.;, ,Özdemir, Z.; at al. Pharmacological Reports, **2019**.
11. Çiftçi, O.; Özdemir Z.; Acar, C.; et al., *Lett. Org. Chem.* **2017**, 15(4), 323-331.
12. Bruel, A.; Loge, C.; Tauzia, M.L.; Ravache, M.; Guevel, R.L.; Guillouzo, C.; Lohier, J.F.; Santos, J.S.O.; Lozach, O.; Meijer, L.; Ruchaud, S.; Bénédetti, H.; Robert, J.M. *Eur. J. Med. Chem*., **2012**, 57, 225-233.
13. Raguenez, G.; Desire, L.; Lantura, V.; Courtois, Y. Biochemical and Biophysical Res. Com. **1999**, 258, 745–751.
14. Banks L, Beard HS, Cao Y, Cho AE, Damm W, Farid R, et al. J Comput Chem **2005**,26,1752–1780.
15. Berman HM, Westbrook J, Feng Z, Gilliland G, Bhat TN, Weissig H, et al.. **2000**,28,235-242.

ITWCCST 2019
5th International Turkic World Conference on Chemical Sciences and Technologies
25 - 29 October, Sakarya / Turkey
2019.itwccst.org

Determination of Zinc Levels in Serum by Using an Electroanalytical Method

Tarik Attar[1,2,*]

[1] *Superior School of Applied Sciences, P.O. Box 165 RP, Tlemcen, 13000, Algeria.*
[2] *Laboratory of ToxicoMed, University of Abou Bekr Belkaïd, Tlemcen, 13000, Algeria.*
att_tarik@yahoo.fr / t.attar@essa-tlemcen.dz

Keywords: Serum, Zinc, Healthy Adults

INTRODUCTION

Zinc is one of the most abundant trace elements in the body [1]. It plays an important role in human growth; it has a recognized action on more than 300 enzymes, by participating in their structure or in their catalytic and regulatory actions [2]. Zinc deficiency is associated with growth retardation, decreased appetite, abnormal wound healing, abnormal sexual function, neurologic abnormality, immune system dysfunction and predisposing to diseases such as diarrhea and pneumonia [3]. Zn with vitamin A participates in many body functions. It is involved in maintenance of immune function in humans [4]. Zinc deficiency has been associated with chronic liver disease, cirrhosis and chronic viral hepatitis [5]. The levels reduced zinc showed an inverse correlation with the degree of liver damage [6], liver fibrosis [7], and markers of liver dysfunction such as bilirubin, albumin, and cholesterol [8]. Serum zinc levels have also been noted in patients with alcoholic cirrhosis [9]. Zinc deficiency is known to adversely influence in immunity and in general health; however, excessive quantities of zinc intake may lead to both chronic and acute toxicity. Age, gender, and geographic location have major effects on zinc status [10]. High level of Zinc is found in Oysters, Red meat, poultry, beans, nuts, certain seafood, whole grains, fortified breakfast cereals, and dairy products. Low level of Zinc is found in vegetable, fruits, tea, coffee, rice, and bread [11].

The differential pulse anodic stripping voltammetry (DPASV) on a hanging mercury drop electrode is a good method for the determination of trace amount of metals in biological samples. The aim of the present study is to introduce DPASV method for the determination of Zinc in serum of healthy adults.

MATERIAL AND METHODS

Apparatus

Anodic stripping voltammetry measurements were performed using a commercially available TraceLab 50 trace analysis system. It consists of POL150 polarographic analyzer, MDE150 polarographic stand and TraceMaster 5 software (Radiometer Analytical S.A, France). The three electrodes system consists of a working hanging mercury dropping electrode (HMDE) that was renewed prior to each measurement, a platinum auxiliary electrode and Ag|AgCl saturated with KCl as reference electrode.

Reagents

All chemicals used were of analytical-reagent grade or the highest purity available. Aqueous solutions were prepared by dissolving a certain amount of chemicals into high-purity deionized water (MilliQ water system). Acids used for the analysis, the nitric acid (69.5%, Fluka) and the perchloric acid (70-72%, Merck). Stock solution of zinc (1000 ppm, atomic adsorption standard, Aldrich) was prepared in deionized water.

Sample digestion

A 0.5 ml of serum blood in a long-necked 50 ml flask, 2.0 mL of acid mixture (1.5 mL HNO_3 and 0.5 mL $HClO_4$) was added in flask. The temperature is maintained with 150°C during 4 hours and then the temperature is fixed at 200°C until quasi total evaporation of the contents [12]. After cooling, we add the same mixture of acids to the residue, then we let evaporate until obtaining a dry residue [13]. This residue is taken again by 5 ml of nitric acid with 0.25% and preserved in polyethylene tubes [14]. Only reagents with low background impurities were used.

Procedure

Ten milliliters of the supporting electrolyte solution were pipetted into the cell and deoxygenated with argon for 5 min. The accumulation potential - 1150 mV was applied to a fresh mercury drop while the solution was stirred. Following the accumulation period, the stirring was stopped and after 5 s the voltammogram was recorded by applying a positive potential scan at 20 mV/s. Each scan was repeated three times with a new drop for each analyzed solution and the mean of these

voltammograms obtained. The operatory conditions for determination of zinc have been optimized by attar et al [15].

RESULTS AND DISCUSSION

Accuracy

The accuracy and precision of the method used were tested in 10 replicate tests with a reference materiel (Seronorm Trace Elements Serum, Billingstad, Norway). It is observed that the precision for two levels is 4.75 and 5.87 %. Furthermore, the percentage recovery of the zinc determination was tested by two levels seronorm with the recommended concentration of zinc are ranging between 96.74 to 105.15% and the accurate for zinc is ranging between 95.67 to 105.17 %. Because of the high sensitivity of the differential pulse anodic stripping voltammetry, this method is applied to the determination of Zinc in the serum. The linear range for zinc was evaluated at 60 s deposition time. The peak current increased linearly with zinc concentration over the range 0.285-57 µg/dL, with correlation coefficient of 0.999 (Figure. 1). The detection limit for zinc was found to be 0.086 µg/dL estimated from 10 replicate determination of blank solution.

Application to serum samples

A total of fifty-five subjects of healthy adults Algerian volunteers were selected in this study. The mean serum zinc concentrations for the healthy adults was 76.57±11.38 µg/dL (Table 1). The Zinc concentration range from 50.14 µg/dL to 129.15 µg/dL in the most of all subjects. As an application the figure below represents a voltammograms relating to the proportioning of zinc in the serum (Figure. 1). The zinc concentration of this sample is equal 69.54 µg/dL.

Table 1. The results of means zinc concentrations, S.D.s, range, and 95% confidence intervals

Mean (µg/dL)	Range (µg/dL)	Confidence 95%
76.57 ± 11.38	50.14 - 129.15	78.12 - 84.71

No significant differences were observed, for zinc in serum concentrations after applying to them the Student's t-test.

The comparison between the mean serum zinc concentration, for the overall samples (76.57±11.38 µg/dL) in the present study, with that of healthy subjects from various countries showed that the mean serum zinc in this study was nearly similar to the mean serum zinc values in healthy subjects of an Turkey study (81.65±16.40 µg/dL) [16] and an Greek study (77.11±17.67 µg/dL) [17].

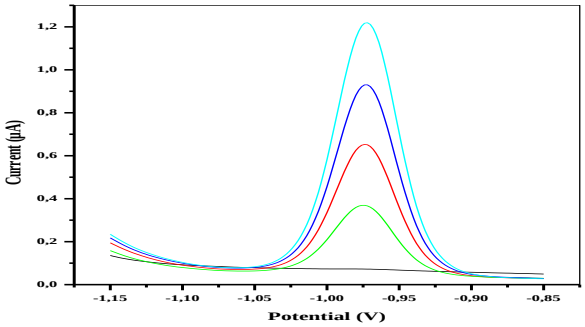

Figure 1. Typical voltammograms for the determination of serum zinc contents in a whole blood sample by the standard addition method.

CONCLUSION

The evaluation of the serum status of Zinc in healthy adults living in the west of Algeria by differential pulse anodic stripping voltammetry was performed for the first time in this study and in general, the results of this study agree with previously reported values from different countries.

ACKNOWLEDGEMENTS

This work was supported by the University of Abou Bekr Belkaid of Tlemcen, Algeria.

REFERENCES

[1] Tapiero H.; Tew KD. Biomed. Pharmacother. **2003**, 57, 399-411.
[2] Jansen J.; Karges W.; Rink L. J. Nutr. Biochem. **2009**, 20, 399-417.
[3] Maret W.; Sandstead HH. J Trace Elem Med Biol. **2006,** 20, 3 -18.
[4]Marjani A.; Mojerloo M.; Mansorian AR.; Golalipour MJ. MJIRC. **2005**, 8, 71–75.
[5] Poo JL.; Rosas-Romero R.; Rodríguez F. Dig. Dis. **1995**, 13, 136–142.
[6] Gür G.; Bayraktar Y.; Ozer D. Hepatogastroenterology. **1998**, 45, 472–476.
[7] Barry M.; Keeling PW.; Feely J. Clin. Sci. **1990**, 78, 547–549.
[8] Pramoolsinsap C.; Promvanit N.; Komindr S. J. Gastroenterol. **1994**, 29, 610–615.
[9] Ijuin H. Kurume. J Med. **1998**, 45, 1–5.
[10] Lachili B.; Faure H.; Arnaud J.; Richard MJ.; Benlatreche C.; Favier A. Int. J. Vitam. Nutr. Res. **2001**, 71, 111 -116
[11] Castillo-Duran C.; Weisstaub G. *J. Nutrit.* **2003**, 133**,** 1494S -1497S.
[12] Attar T.; Larabi L. Der. Pharma. Chemica. **2011**, 3, 400-405.
[13] Attar T.; Harek Y.; Medjati N.; Larabi L.; Inter. J. Anal. Bioana. Chem. **2012**, 160-164.
[14]Attar T.; Larabi L.; Harek Y. Med. J. Chem. **2014**, 6, 691-700.
[15]Attar T.; Larabi L.; Harek Y. J. Adv. Chem. **2013**, 6, 855-860.
[16] Vural H.; Uzun K.; Kocyigit A.; Hgli A.; Akyol O. Trace. Elem. Med. Biol. **2000**, 14, 88-91.
[17] Kouremenou-Dona E.; Dona A.; Papoutsis J.; Spiliopoulou C. Sci. Total. Environ. **2006**, 359, 76-81.

ITWCCST 2019
5th International Turkic World Conference on Chemical Sciences and Technologies
25 - 29 October, Sakarya / Turkey
2019.itwccst.org

Effect of Boron Nitride Concentration: Synthesis and Characterization of Boron Nitride Nanosheets (BNNSs) Exfoliated in Water

Gizem Sezer[1], Duygu Kuru[1], Alev Akpinar Borazan[1,*]

[1]*Bilecik Seyh Edebali University, Chemical Engineering Department, Gülümbe, 11210, Bilecik*

alev.akpinar@bilecik.edu.tr

Keywords: Boron nitride, boron nitride nanosheet, exfoliation, sodium dodecylsulfate

INTRODUCTION

While layered nanomaterials or two-dimensional nanomaterials are defined as materials with relatively large lateral dimensions and strong chemical bonds, the ability to form less layered and weaker Van der Waals bonds is an active research area. Hexagonal boron nitride (h-BN) is still one of the two-dimensional nanomaterials whose research is continuing[1]. So far, several methods for synthesizing 2D h-BN have been developed. Similar to graphene, 2D h-BN can be produced by mechanical or chemical exfoliation. The methods of producing boron nitride nanosheets (BNNSs) are generally those which can be classified as a bottom-up approach that forms a two-dimensional nanosheet by incorporating small molecules or precursors into complex nanostructures. In contrast, the exfoliation approach creates a 2D nanosheet starting from bulk materials that can be classified as a top down method[2]. In a study conducted by Wang et al. boron nitride nanosheets were produced by exfoliation on a large scale in methane sulfonic acid. BNNSs were produced for the first time by liquid phase exfoliation of h-BN particles in methane sulfonic acid. Researchers have reported that such sulfonic acid is more potent against exfoliation and stabilization of BNNS compared to commonly used organic solvents. They concluded that the yield of the product in methane sulfonic acid solution could reach up to 0.3 mg/mL[3]. Zhi and colleagues in their study have made large-scale synthesis of BNNSs. N, N-dimethylformamide (DMF), a strong polar solvent, was used. The researchers increased the mechanical strength of composites by 22% by using BNNSs in composite production[4]. In this study, BNNSs were prepared at different concentrations and various characterization procedures were performed. Boron nitride powder (micron size,> 98% purity, Bortek Bor Teknolojileri ve Mekatronik San. Tic. A.Ş.) was used to form BNNSs. Deionized water was used as solvent in the preparation of the suspension. Sodium dodecyl sulfate (SDS, Sigma Aldrich, 98.5%) was used as the surface activator to ensure effective distribution of boron nitride in water. Boron nitride nanosheets were synthesized by a method known as liquid exfoliation. In Figure 1 schematic diagram of BNNSs synthesis were given.

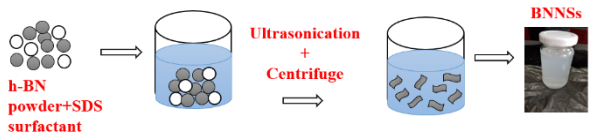

Figure 1. Synthesis of BNNSs

Mixtures prepared at different initial concentrations (0.2, 0.6, 0.8, 1.0, 1.2, 1.4, 1.6, 1.8 and 2mg/mL) were sonicated in a 180 W ultrasonic bath at 45 minutes intervals for 6 hours. SDS was added at 0.1% by weight. In order to control the bath temperature, cold water circulation was provided by creating an ice bath in the ultrasonic bath. When cold water circulation was stopped during sonication, the temperature rose to 60°C within a few hours due to the spread of sonic energy. When the ice bath was repeated every 30 min, the temperature was maintained at 30°C. Boron nitride was centrifuged at 6000 rpm for 30 minutes to remove unexfoliated BN particles.

Efficiency analysis of the obtained nanosheets was determined by UV visible region spectroscopy (Agilent Technologies, Cary 60 UV-Vis). Morphological image of nanosheets prepared at different concentrations was examined by Scanning Electron Microscopy (SEM, Zeiss Supra 40VP, Germany) analysis. The presence of boron nitride and other groups in boron nitride nanosheets was investigated by FT-IR (Agilent Technologies, Cary 630 FTIR) analysis. Raman analysis proved the exfoliated boron nitride layers. AFM analysis showed the thickness of BNNSs.

RESULTS AND DISCUSSION

FT-IR analyzes were performed in the wavenumber range of 400-4000 cm^{-1}. The boron nitride nanosheets prepared at different concentrations were coated onto the copper layer and the analysis was performed. Figure 2 shows the IR spectra of boron nitride nanosheet suspensions at different concentrations.

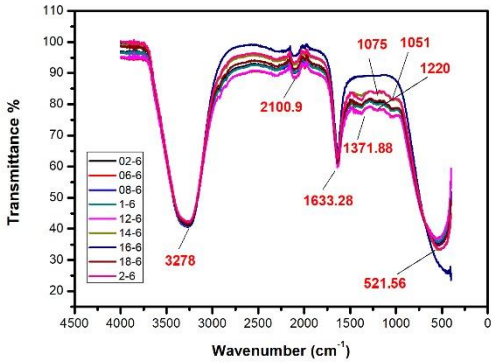

Figure 2. IR spectra of boron nitride nanosheet suspensions prepared at different concentrations

IR spectra of boron nitride nanosheet suspensions prepared at different concentrations are similar when examined in Figure 2. The stress at 3278 cm^{-1} wavenumbers seen in all samples refers to the H-OH strain from the sodium dodecyl sulfate structure. The peak at a wavenumber of 2100,9 cm^{-1} belongs to strong C-C binding. Again, the sharp stress at the wavenumber of 1633 cm^{-1} belongs to amide C = O binding[5]. It was evaluated that the stress occurring in 1371.88 cm^{-1} belongs to the characteristic B-N-B binding mode and B-N stress in the structure of boron nitride [6-8]. The peak at 1075 cm^{-1} is the stress caused by C-C binding. At 1051 cm^{-1} wavenumber, the peak of the C-O-C stretch is seen. It contains the skeleton vibration bridge caused by peak S-O stretching at a wavenumber of 1220 cm^{-1}. Wide band tension of 521,56 cm^{-1} wavenumber occurred as a result of C-H asymmetric stress[5].

The surface to be imaged was coated with palladium/ gold before SEM analysis. Boron nitride nanosheet suspensions prepared at different concentrations were plated onto copper layer by drop casting method and morphological images were taken at 30.00 Kx magnification by SEM analysis. Most of the h-BNs were thick flakes of lateral dimensions ranging from one hundred nanometers to several micrometers. As the boron nitride concentration increased, boron nitride layers were deposited on top of each other (Figure 3-h, i). At low concentrations, exfoliation and separation are more visible (a, b, c). The stripping of the nanoparticles in the solvent occurs due to the strong interaction between the solvent and the nanoparticles; this means that the energy for exfoliation is low. This energy for the water solvent is generally low compared to different solvents and surfactants such as SDS are used to obtain boron nitride in thin layers[9].

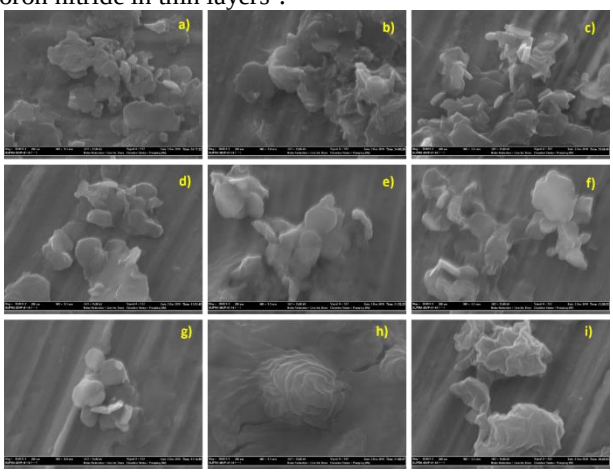

Figure 3. SEM images of boron nitride nanosheet suspensions prepared at different concentrations a) 02-6 b) 06-6 c) 08-6 d) 1-6 e) 12-6 f) 14-6 g) 16-6 h) 18-6 i) 2-6

During sonication of boron nitride flakes in the solvent, initially large flakes are divided into smaller flakes, and as time increases, more energy is given to yield small amounts of layers or high concentration monoslides [10].

UV-Visible Spectrophotometer was used to calculate the concentration values of boron nitride nanosheets. Boron nitride suspensions were prepared using deionized water at concentrations of 0.01, 0.02, 0.03, 0.04, and 0.05 mg / mL and absorbance values at 400 nm wavelength were noted. The absorbance values corresponding to the concentration values were plotted and a calibration curve was generated (Figure 4). The amount of boron nitride nanosheets obtained at different initial concentrations was determined using the calibration curve equation (y = 7.831x + 0.01629). Table 1 shows the absorbance values, concentration amounts and % yields of nanosheets obtained at different concentration values.

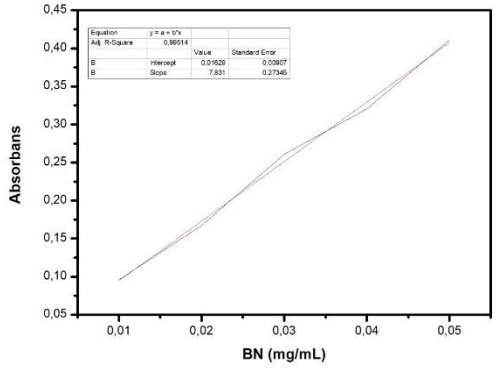

Figure 4. Boron nitride-water suspension calibration curve

Table 1. Absorbance and concentration values of boron nitride nanosheets synthesized at different concentration values

Sample Codes	Absorbance	Concentration (mg/mL)	Yield %
02-6	0.1357	0.0152	7.60
06-6	0.1112	0.0121	2.01
08-6	0.1803	0.0209	2.61
1-6	0.1080	0.0117	1.60
12-6	0.1676	0.0193	1.17
14-6	0.0690	0.0067	0.48
16-6	0.1888	0.0220	0.32
18-6	0.0445	0.0036	0.20
2-6	0.0520	0.0046	0.23

When the results calculated according to the calibration curve were examined, concentration values varied between 0.003 and 0.02 mg/mL. According to the results, when the initial concentration was increased to 1.8 and 2 mg/mL, the yield decreased considerably. These results are in parallel with SEM analysis. In the nanosheet images obtained at high concentration values, boron nitride layers were deposited on top of each other (Figure 3-h, i). At low concentrations, exfoliation and separation are more visible (a, b, c). This affected the yields of the obtained nanosheets. The highest yield was 7.60% at an initial concentration of 0.2 mg/mL.

Raman analysis was performed to obtain boron nitride nanosheets formation. Raman spectrum belongs to 08-6 sample was given in Figure 5. The characteristic peak of BNNSs was seen in Raman spectra at 1366.51 cm^{-1}. The stress of the E2g vibration mode shows a shift in nanosheets relative to the bulk form in the structures. This is due to the reduction in the particle size of the boron nitride and the separation of the structure into layers. As the number of layers increases, the E2g band shifts to the right. In the study of Thripuranthaka et al., Raman spectra of nanosheets consisting of bulk h-BN powder, single layer nanosheet and several layers were compared. When the spectra were examined, the Raman peak of h-BN was observed at 1359,32 cm^{-1}, the single-layer nanosheet peak was 1361,14 cm^{-1}, and the multiple-layer nanosheet peak was 1366,48 cm^{-1}. When the results were examined, Raman peaks shifted to right in the spectrum in the transition from bulk form to multilayer nanosheet form[11].

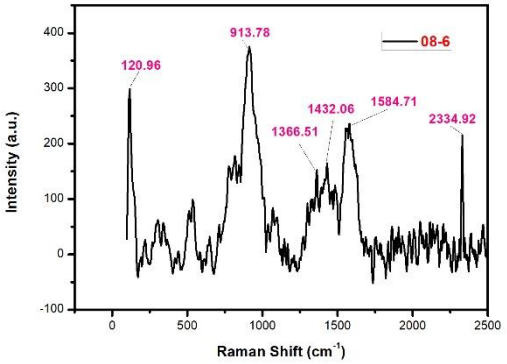

Figure 5. Raman spectrum of 08-6 sample

Figure 6 shows the AFM image of 08-6 sample. AFM analysis was performed to obtain the thickness of the nanosheets.

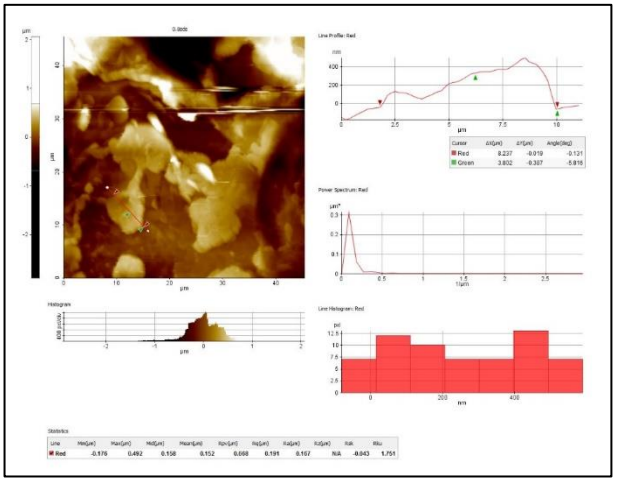

Figure 6. AFM histogram of 08-6 sample

In Figure 6, the thickness of nanosheets varies between 0-400 nm. Here, darker parts represent thicker layers, while light colored nanosheets represent thinner layers. Thick nanosheets are also observed due to the formation of overlapping nanosheets as a result of agglomeration due to a single layer coating on the silicon wafer. The AFM histogram is parallel to the SEM images. When examined in Figure 3-c, nanosheets are in agglomerated form. Excessive use of SDS surfactant resulted in agglomeration of nanosheets instead of stratification.

CONCLUSION

The IR spectra of boron nitride nanosheet suspensions prepared at different concentrations yielded similar peaks. The H-OH bond of sodium dodecyl sulfate used as the surface activator, strong C-C binding, C = O binding to the amide, C-O-C and S-O binding resulted in C-H asymmetric stretching. The characteristic B-N-B

binding mode and B-N stress in the structure of boron nitride were also observed in the spectrum.

Most of the h-BNs were thick flakes of lateral dimensions ranging from one hundred nanometers to several micrometers. When SEM images were examined, as boron nitride concentration increased, boron nitride layers were deposited on top of each other. At low concentrations, exfoliation is better.

Yield increased considerably when the initial concentration was increased to 1.2 and 1.6mg/ mL. These results are in parallel with SEM analysis. The highest yield was obtained with an initial concentration of 0.2 mg/mL at 7.60%.

The raman spectrum proved that boron nitride was separated into layers. E2g vibration mode shows a shift in nanosheets relative to the bulk form in the structures.

Excessive use of SDS surfactant resulted in agglomeration of nanosheets instead of stratification.

ACKNOWLEDGEMENTS

We would like to thank Bilecik Şeyh Edebali University Scientific Research Projects Unit, who supported our work with the project of 2018-01.BŞEÜ.03-06.

REFERENCES

[1] Bhimanapati, G.R.; Kozuch, D.; Robinson, J.A. Nanoscale. **2014,** 6, 11671-11675.
[2]Ansoloni, L.M.S. Mater. Sci. Appl. **2013,** 4, 22-28.
[3] Wang, Y.; Shi, Z.; Yin, J. J. Mater. Chem. **2011,** 21, 11371-11377.
[4] Zhi, B.C.; Bando, Y.; Tang, C.; Kuwahara, H.; Golberg, D. Adv. Mater. **2009,** 21, 2889-2893.
[5] Singh, M.K.; Agarwal, A.; Gopal, R.; Swarnkar, R.K.; Kotnala, R.K. J. Mater. Chem. **2011,** 21, 11074-11079.
[6] Wang, L.; Sun, C.; Xu, L.; Qian, Y. Catal. Sci. Technol. **2011,** 1, 1119-1123.
[7] Hou, J.; Li, G.; Yang, N.; Qin, L.; Grami, M.E.; Zhang, Q.; Wang, N.; Qu, X. RSC. Adv. **2014,** 4, 44282-44290.
[8] Yu, B.; Xing, W.; Guo, W.; Qui, S.; Wang, X.; Lo, S.; Hu, Y. J. Mater. Chem. A. **2016,** 4, 7330-7340.
[9] Liu, J.; Kutty, R.G.; Zheng, Q.; Eswariah, V.; Sreejith, S.; Liu, Z. Small. **2016,** 13, 1602456.
[10] Durge, R.; Kshirsagar, R.V.; Tambe, P. Procedia Engineering. **2014,** 97, 1457-1465.
[11] Thripuranthaka, M.; Rout, C.S.; Late, D.J. Mater. Res. Express. **2014,** 1, 035038.

ITWCCST 2019
5th International Turkic World Conference on Chemical Sciences and Technologies
25 - 29 October, Sakarya / Turkey
2019.itwccst.org

Two-dimensional Hexagonal Boron Nitride Nanosheets Grown by Surfactant-added Exfoliation

Serra Başoğlu[1], Duygu Kuru[1], Alev Akpinar Borazan[1,*]

[1]Bilecik Seyh Edebali University, Chemical Engineering Department, Gülümbe, 11210, Bilecik

alev.akpinar@bilecik.edu.tr

Keywords: 2-D materials, boron nitride nanosheet, ionic surfactant, liquid exfoliation.

INTRODUCTION

Recent advances in understanding graphene crystals in two-dimensional (2D) order have encouraged more researchers to work in the field of nanosheets. 2D materials have a regular structure. In these materials, atoms are contained within a single layer. There are no different layers with strong or weak bonds between them [1]. The best known 2D material is graphene[2] which is the thinnest material known to date, as a single layer of a carbon honeycomb weave. Based on composition and crystal structure, many other 2D materials are known to have been predicted and synthesized in the last decade [3-6]. These materials have an ultra-thin layer structure but have different functions for different applications. Undoubtedly, because of the large number of 2D materials, their unique properties and their versatility, scientists and engineers have become interested in a wide range of research. Electronics, optoelectronics, energy storage and conversion, etc. are promising applications for 2D materials[7]. There are several methods for producing 2D materials. The best known is the micro mechanical division (MC)[2] which uses Scotch tape to separate thin layers from bulk material. Chemical vapor deposition method (CVD) is a well-known method for synthesizing nanomaterials containing zero-dimensional (OD), one-and two-dimensional (1D and 2D) materials in large quantities based on the bottom-up production principle[1]. Because of the nature of the layered nanomaterials, that is, they have strong in-plane covalent bonds between the structural components and weak van der Waals interaction between the atomic layers, it is possible to directly synthesize 2D nanosheets by exfoliation method based on 3D crystals[8].

Since boron nitride nanosheets do not effectively disperse in water, some surfactants are used for the exfoliation process. However, the concentration and lateral size of nanosheets in aqueous BNNS dispersions are quite low. To increase BNNSs concentration, ionic surfactants may be used in liquid exfoliation. At the same time, ionic surfactants provide both advantages such as effective shielding of BNNS from water and good dispersibility with water that allows it to preferably migrate to the BNNS surface and provide suspension stability[9]. Lotya et al. used SDBS ionic surfactant to produce graphene in water solution using ultrasonication technique. They successfully synthesized multilayer graphene smaller than 5 layers. They also proved that surfactant added dispersions were stable for 6 weeks[10].

Smith et al. reported the effect of 12 different ionic and non-ionic surfactant addition on production of graphene nanosheets in water suspension. For all surfactants the similar flake size obtained, and the dispersed concentration varied by a factor of 2-3 from surfactant to surfactant. It was also mentioned that ionic surfactants stabilized the sheets and played an important role to protect nanosheets from aggregation[11].

In the current paper, three kind of surfactant such as sodium dodecylsulfate (SDS) powder, sodium dodecyl benzene sulfonate (SDBS) and deoxyclic acid (DA) were used in the synthesis of boron nitride nanosheets using liquid exfoliation method. Specific ratios of surfactants and boron nitride powder were ultrasonically dispersed in water and centrifuged to form BNNSs.

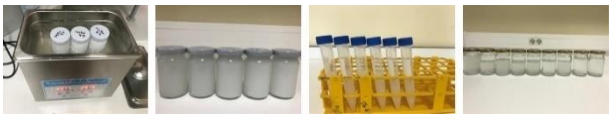

Figure 1. Ultrasonic-centrifuge technique for BNNSs production

In Figure 1 ultrasonic-centrifuge technique for BNNSs production was given. In this method, BNNSs were produced based on 5 different initial concentrations (0.2, 0.6, 0.8, 1.2, and 1.6). 3 different surfactants and boron nitride were combined to a certain extent and sonicated in an ultrasonic bath for 6 hours. It was centrifuged at 6000 rpm for 30 minutes to remove undesirable boron nitride particles. The efficiency analysis of the obtained nanosheets was determined by

UV visible region (Agilent Technologies, Cary 60 UV-Vis) spectroscopy. The morphological structure of nanosheets and surfactants was investigated by Scanning Electron Microscope (SEM, Zeiss Supra 40VP, Germany) analysis. Formation of boron nitride was proved with FT-IR (Agilent Technologies, Cary 630 FTIR) and Raman analysis. The thickness distribution of boron nitride nanosheets was determined by AFM analysis.

RESULTS AND DISCUSSION

UV-Visible Spectrophotometer was used to calculate the concentration values of boron nitride nanosheets. Table 1 shows the yield of boron nitride nanosheets after exfoliation with different surfactants.

Table 1. Concentration and yield values of boron nitride nanosheets synthesized with different surfactants

Initial concentration (mg/mL)	Surfactant	Concentration of BNNSs (mg/mL)	Yield %
0.2	SDS	0.0152	7.60
0.6	SDS	0.0121	2.01
0.8	SDS	0.0209	2.61
1.2	SDS	0.0193	1.60
1.6	SDS	0.0220	1.38
0.2	SDBS	0.0015	0.75
0.6	SDBS	0.0122	2.03
0.8	SDBS	0.0198	2.48
1.2	SDBS	0.0268	2.23
1.6	SDBS	0.0144	2.55
0.2	DA	0.0008	0.40
0.6	DA	0.0064	1.06
0.8	DA	0.0025	0.31
1.2	DA	0.0058	0.48
1.6	DA	0.0104	0.65

When the yield results of BNNSs produced using SDS surfactant were examined, concentration values varied between 0.01 and 0.02 mg/mL. These results are in parallel with SEM analysis. In the nanosheet images obtained at high concentration values, boron nitride layers were deposited on top of each other (Figure 2-d, e). At low concentrations, exfoliation and separation can be seen clearly (a, b, c). This affected the yields of the obtained nanosheets. When SDBS surfactant is used, boron nitride yields are between 0.75 and 2.5%. It was observed that the yields were lower when compared with SDS surfactant. In DA surfactant, yield results were significantly lower than both SDS and SDBS (0.3-1.06%). Figure 2,3 and 4 shows the SEM images of BNNSs with different surfactants.

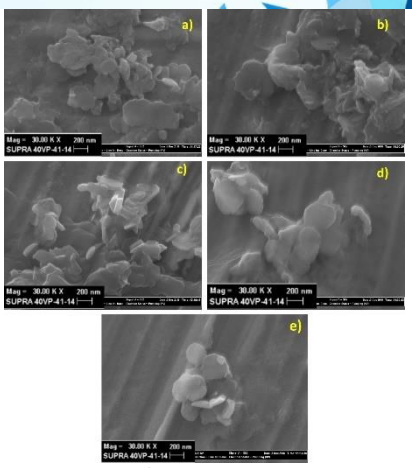

Figure 2. SEM images of boron nitride nanosheet suspensions prepared with SDS surfactant a) 02-6 b) 06-6 c) 08-6 d) 12-6 e) 16-6

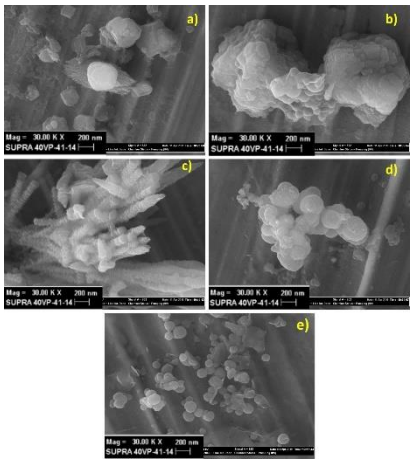

Figure 3. SEM images of boron nitride nanosheet suspensions prepared with SDBS surfactant a) 02-6 b) 06-6 c) 08-6 d) 12-6 e) 16-6

When the morphological images of BNNSs obtained using 3 different surface activators are examined, it is possible to say that SDBS is the most effective surfactant in layer-by-layer separation of boron nitride. Exfoliated layers of boron nitride were observed, especially when the initial concentration of 1.6 mg/mL was used (Figure 3-e). In Figure 3, as the initial concentration is increased, the formation of boron nitride nanosheet is more pronounced. At low concentrations, BNNSs attached to the SDBS surfactant are observed (Figure 3-c). In order to stabilize the produced 2D nanosheets, the interfacial tension between the materials and the liquid medium needs to be minimized, thus reflecting the existence of good interactions[12].

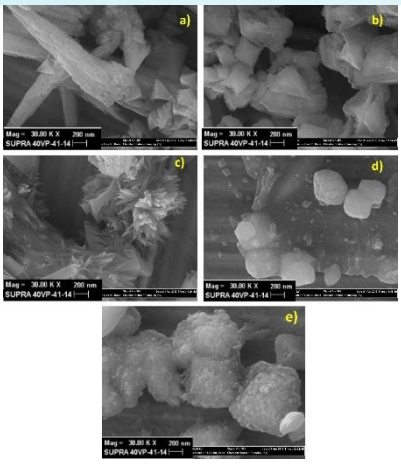

Figure 4. SEM images of boron nitride nanosheet suspensions prepared with DA surfactant a) 02-6 b) 06-6 c) 08-6 d) 12-6 e) 16-6

Figure 4 shows the typical morphological structure of the DA surfactant (Figure 4-a). It was not effective in separating boron nitride as a layer in all studied concentrations. When the efficiency results of the DA surface activator are examined, it can be said that they are in parallel with the morphological images.

Raman analysis was performed to prove the formation of BNNSs. Figure 5 shows the Raman spectra of BNNSs produced by using SDS, SDBS and DA surface activators. According to the SEM images three samples (08-SDS, 16-SDBS and 12-DA) were chosen for Raman analysis.

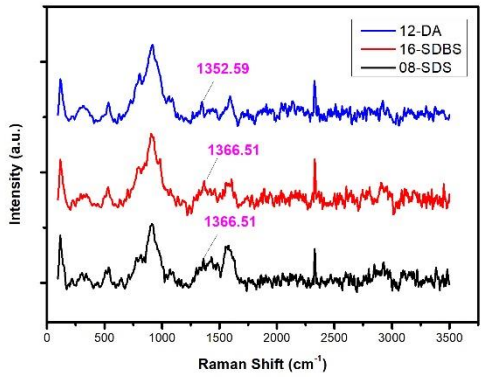

Figure 5. Raman spectra of BNNSs prepared with different surfactants

Raman spectroscopy is widely used for the characterization of lattice vibration modes of graphene-based materials. Considering shear, width and ratio between different peaks, Raman results can show the quality, layers and defect density of graphene-based materials. The typical E2g band of h-BN is about 1365 cm^{-1}; this is 1055 cm^{-1} for transverse phonons and 1305 cm^{-1} for longitudinal cubic BN [13].

This reduction in Raman density of E2g vibration can be attributed to poor interaction between layers due to exfoliation in the solvent. (002) the slight shift of the peak to the right is also associated with increased layer voids after exfoliation [14]. As the number of layers increases, the E2g band shifts to the right. From Figure 5 we can conclude that BNNSs produced with SDS and SDBS surfactants have more layers compared with the DA one as the E2g band seems at 1366.51 cm^{-1} while DA surfactant has E2g band at 1352.59 cm^{-1}.

The variation in Raman density may claim that due to the less controllable sample quantity under the irradiation of the laser spot, it may not accurately reflect the number of layers. However, the rational exfoliated BNNSs have less bulk density than h-BN bulk materials due to the greater space between the layers. In addition, increased imperfections and edge effects after exfoliation of BNNS can also be considered as the causes of E2g band change [15].

Figure 6 includes the AFM histograms of BNNSs. From Figure 6-a the thickness of nanosheets varies between 40-100 nm. The lateral dimension ranges between 1-2.5 µm.

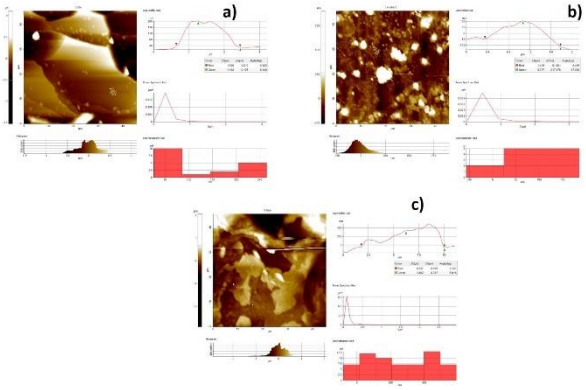

Figure 6. AFM histogram of BNNSs produced with different surfactant a) DA, b)SDBS, c)SDS

In Figure 6-b we can say that BNNSs produced with SDBS surfactant have thickness range between 0-100 nm and lateral size range is 0.4-1.8 µm. For the surfactant of SDS the thickness of BNNSs range between 0-400 nm while lateral size reaches to 10 µm. If we compare all kind of BNNSs produced with different surfactant, DA and SDBS have thinner nanosheets. BNNSs produced with SDS are thick and their lateral size is also bigger than the others.

IR spectra of boron nitride nanosheet suspensions prepared with different surfactants are similar when examined in Figure 7-9.

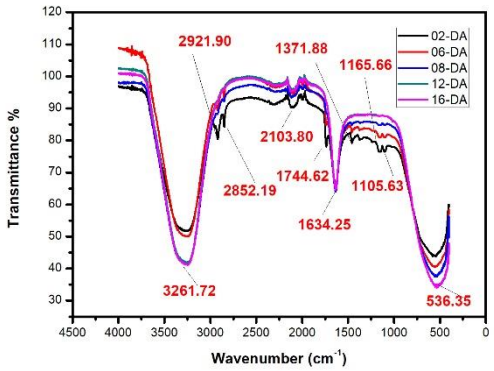

Figure 7. IR spectra of boron nitride nanosheet suspensions prepared with DA surfactant

When IR spectra are examined, it is observed that as boron nitride concentration increases, boron nitride band narrows. The stress at 3261.72 cm^{-1} wavenumbers seen in all samples belongs to the H-OH strain from the DA, SDBS and SDS structure. The peak at 2116,39 cm^{-1} belongs to strong C-C binding. Again, the sharp stress at the wavenumber of 1634.25 cm^{-1} refers to amide C = O binding[3]. It was evaluated that the stress occurring in 1371.88, 1373.88, 1377.68 belongs to the characteristic B-N-B binding mode and B-N stress in the structure of boron nitride [16]. The peak at 1165.66 cm^{-1} is the stress caused by C-C binding. At 1105.63 cm^{-1} wavenumber, the peak of the C-O-C stretch is seen. It contains the skeleton vibration bridge caused by peak S-O stretching at a wavenumber of 1220 cm^{-1}. Wide band tension of 536.35 cm^{-1} wavenumber occurred as a result of C-H asymmetric stress[3].

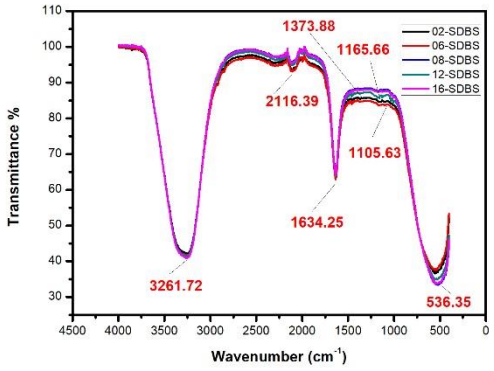

Figure 8. IR spectra of boron nitride nanosheet suspensions prepared with SDBS surfactant

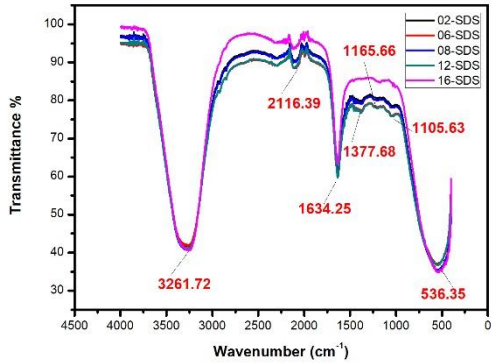

Figure 9. IR spectra of boron nitride nanosheet suspensions prepared with SDS surfactant

CONCLUSION

If the results are summarized:

- DA surfactant was not effective in separating boron nitride as a layer in all studied concentrations. According to the SEM images SDBS showed better performance as a surface activator.
- In DA surfactant, yield results were significantly lower than both SDS and SDBS (0.3-1.06%).
- The ramectrum proved that boron nitride was separated into layers. We can conclude that BNNSs produced with SDS and SDBS surfactants have more layers compared with the DA one as the E2g band seems at 1366.51 cm^{-1} while DA surfactant has E2g band at 1352.59 cm^{-1}.
- AFM histogram shows us DA and SDBS have thinner nanosheets. BNNSs produced with SDS are thick and their lateral size is also bigger than the others.

ACKNOWLEDGEMENTS

We would like to thank Bilecik Şeyh Edebali University Scientific Research Projects Unit, who supported our work with the project of 2018-01.BŞEÜ.03-06.

REFERENCES

[1] Tan, C.; Cao, X.; Wu, X.; He, Q.; Yang, J.; Zhang, X.; Chen, J.; Zhao, W.; Han, S.; Nam, G.; Sindoro, M.; Zhang, H. Chem. Rev. **2017,** 117, 6225-6331.
[2] Novoselov, K.S.; Geim, A.K.; Morozov, S.V.; Jiang, D.; Zhang, Y.; Dubonos, S.V.; Grigorieva, I.V.; Firsov, A.A. Science. **2004,** 306, 666-669.
[3] Nicolosi, V.; Chhowalla, M.; Kanatzidis, M.G.; Strano, M.S.; Coleman, J.N. Science. **2013,** 340, 1226419-18.
[4] Ma, B.R.; Sasaki, T. Adv. Mater. **2010,** 22, 5082-5104.
[5] Wang, Q.H., Kalantar-Zadeh, K.; Kis, A.; Coleman, J.N.; Strano, M.S. Nat. Nanotechnol. **2012,** 7, 699-712.
[6] Geim, A.K.; Grigorieva, I.V. Nature. **2013,** 499, 419-425.

[7] Cai, X.; Jiang, Z.; Zhang, X.; Zhang, X. Nanoscale. Res. Lett. **2018,** 13, 241.
[8] Wang, Z.; Tang, Z.; Xue, Q.; Huang, Y.; Huang, Y.; Zhu, M.; Pei, Z.; Li, H.; Jiang, H.; Fu, C.; Zhi, C. Chem. Rec. **2016,** 16, 1204- 1215.
[9] Habib, T.; Devarajan, D.S.; Khabaz, F.; Parviz, D.; Achee, T.; Khare, R.; Green, M.J. Langmuir. **2016,** 32, 1-23.
[10] Lotya, M.; Hernandez, Y.; King, P.J.; Smith, R.J.; Nicolosi, V.; Karlsson, L.S.; et al. J. Am. Chem. Soc. **2009,** 131,3611-20.
[11] Smith, R.J.; King, P.J.; Lotya, M.; Wirtz, C.; Khan, U.; De, S.; et al. Adv. Mater. **2011,** 23, 3944-8.
[12] Backes, C.; Smith, R.J.; McEvoy, N.; Berner, N.C.; McCloskey, D.; Nerl, H.C.; et al. Nat Commun. **2014,** 5,4576.
[13] Lin, Y.; Connell, J.W. Nanoscale. **2012,** 4, 6908-6939.
[14] Lin, Y.; Bunker, C.E.; Shiral Fernando, K.A.; Connell, J.W. Acs. Appl. Mater. Inter. **2012,** 4, 1110-1117.
[15] Song, L.; Ci, L.; Lu, H.; Sorokin, P.B.; Jin, C.; Ni, J.; Kvashnin, A.G.; Kvashnin, D.G.; Lou, J.; Yakobson, B.I.; Ajayan, P.M. Nano. Lett. **2010,** 10, 3209.
[16] Hou, J.; Li, G.; Yang, N.; Qin, L.; Grami, M.E.; Zhang, Q.; Wang, N.; Qu, X. RSC. Adv. **2014,** 4, 44282-44290.

ITWCCST 2019
5th International Turkic World Conference on Chemical Sciences and Technologies
25 - 29 October, Sakarya / Turkey
2019.itwccst.org

Investigation of Valproic Acid-Sensitive Biosensor Used in the Treatment of Epilepsy

Ömer Işıldak[1], Oğuz Özbek[1], Esra Özkan[2]

[1]*Tokat Gaziosmanpaşa University,Faculty of Science and Arts, Department of Chemistry, 60250 Tokat*

[2]*Tokat State Hospital, Department of Neurology,60100 Tokat*

omer.isildak@gop.edu.tr

Keywords: epilepsy, anti-epileptic, valproic acid, biosensor

INTRODUCTION

Biosensors are analytical devices that convert a biological response into an electrical signal. biosensors must be highly specific, and independent of pH, temperature and other physical parameters. In addition should be reusable. [1]. Biosensor technology is based on a specific biological recognition element (enzyme, microorganism etc) in combination with a transducer for signal processing. Biosensors have been play a significant role in medicine, agriculture, food safety, environmental and industrial monitoring [2-5].

Epilepsy is the one of the most common neurological disorder and affects people of all ages. Epilepsy is characterized by unpredictable seizures and can cause different health problems. Epileptic seizures are caused by disturbances in the electrical activity of the brain. Epilepsy is a long-term illness and its medicines are the mainstay of epilepsy treatment and sometimes the use of lifetime anti-epileptic is required. Therefore, the side effects of short and long-term treatment should be taken into consideration as well as efficacy in the treatment chosen and follow-up during use is important. Valproic acid (sodium valproate) is one of the most effective and broad-spectrum anti-epileptic drugs in epilepsy treatment. Furthermore it is one of the most widely used anti epileptics worldwide and its use is increasing day by day. Valproic acid pharmacological effects involve increased gamma-aminobutyric acid reduced release and/or effects of excitatory amino acids, blockade of voltage gated sodium channels [6].

To maintain the therapeutic blood concentration, in patients who use valproic acid, valproic acid test is performed which determine the amount of drug in the bloodstream. The normal value range of valproic acid in the blood is 50 - 100 µg / ml. If the level of blood in the drug is below this range, adequate therapeutic efficacy cannot be achieved. On the contrary, if the drug concentration in bloodstream is increases, which will cause more harm than good. In higher concentration the drug results to toxic and unwanted adverse side effects. Generally, if the level of sodium valproate is within the therapeutic limits, the patient does not have seizure recurrences, mood swings, or significant side effects in the patient and indicates that the patient uses adequate amounts of valproic acid.

This work proposal is presented for the purpose of completing a number of preliminary studies to develop a biosensor in order to follow the drug level in the blood of patients using valproic acid in the treatment of epilepsy.

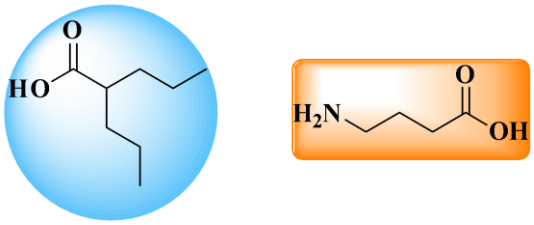

Figure 1. Structure of valproic acid and gamma-amino butyric acid (GABA)

RESULTS AND DISCUSSION

The valproic acid-selective electrode was evaluated potentiometric performance for optimize electrode composition. Valproic acid selective electrode was determined calibration curve of the over sodium valproate concentration range of 1.0 x 10^{-1} to 1.0 x 10^{-5} M.

The optimum electrode was prepared by thorough mixing of 5.5 % ionophore (gamma aminobutyric acid), 55.0 % graphite and 39.5 % epoxy in 5 mL of THF. This mixture was placed on the electrodes surface and let dry for 24 h. Prior to first use, the prepared electrodes were conditioned in a 1.0 x 10^{-2} M sodium valproate solution for 6 h. Preparation of other membranes and optimized of membrane ingredients are summarized Table 1.

Figure 1 and 2 clear that the best valproic acid selective electrodes exhibited a linear response, the graph of the linear response was defined by the equation of E = –7,786 (-log [VPA]) + 1298,8 and -19,472 (-log [VPA]) + 1087,4 with a correlation coefficient r^2 = 0.9996 and r^2 = 0,990.

Table 1. Optimized of electrode ingredients

No	Composition (% w/w)			
	GABA	**Graphite**	**Epoxy**	***R*²**
1	4.5	50.0	45.5	0.9827
2	5.5	50.0	44.5	0.9864
3	**5.5**	**55.0**	**39.5**	**0.9942**
4	6.0	50.0	44.0	0.9900
5	7.0	50.0	43.0	0.9844
6	8.0	50.0	42.0	0.9808

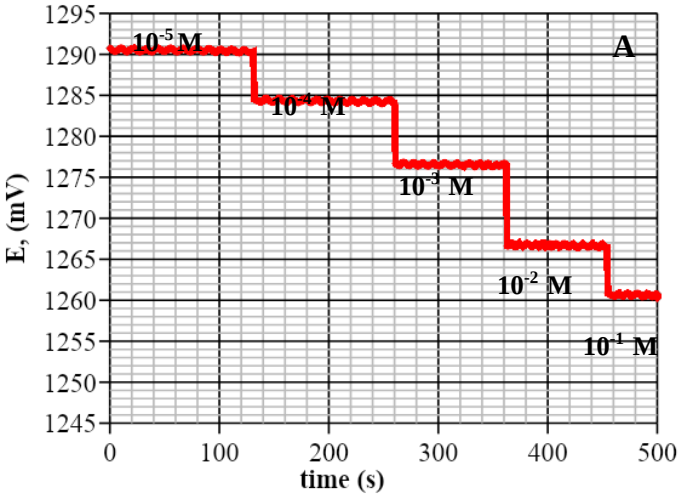

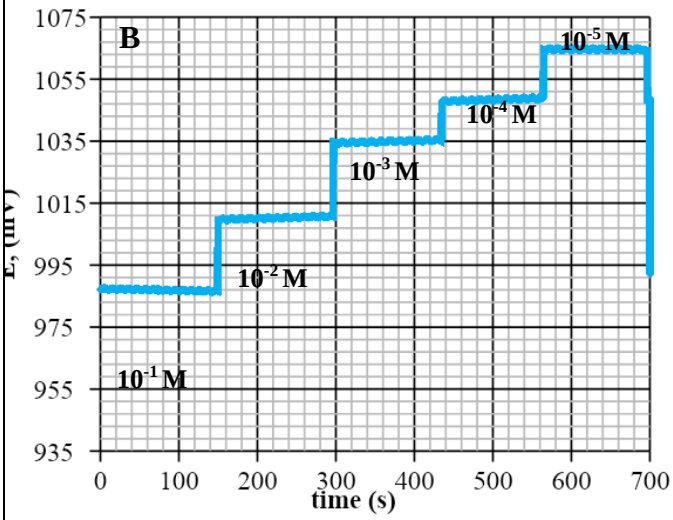

Figure 1 (A-B). Potentiometric response of the best valproic acid selective electrodes against 1.0 x 10^{-1} – 1.0 x 10^{-5} M sodium valproat ion

CONCLUSION

In this study, a potentiometric electrode which is sensitive and selective for the determination of sodium valproate in aqueous solutions was developed. The best valproic acid selective electrode exhibited a linear response (E = –7.786 (-log [VPA]) + 1298,8 and r^2 = 0.9969) concentration range of 1.0 x 10^{-1} to 1.0 x 10^{-5} M sodium valproate ions. The electrode has been shown to have good reusability (10^{-2} to 10^{-4} M sodium valproate ion solution), and fast response time of approximate 10 second.

REFERENCES

[1]Mehrotra, P. J. Oral Biol. Craniofac. Res. **2016**, 6(2), 153–159.
[2]Singh, M.; Verma, N.; Garg, A. K.; Redhu, N. *Sensors and Actuat. B*, **2008**, 134, 345-351.
[3]Gronow, M. Biosensors, *Trends Biochem. Sci.* **1984**, 9(8), 336–340.
[4]Luong, J. H. T.; Mulchandani, A.; Guilbault, G. G. *Trends Biotechnol*. **1988**, 12(6), 310-316.
[5]Luong, J. H. T.; Male, K. B.; Glennon, J. D. *Biotechnology Adv.* **2008**, 26, 492-500.
[6]Fagundes, S. B. R. Rev. Neurocienc. **2008,** 16(2), 130-136.

ITWCCST 2019
5th International Turkic World Conference on Chemical Sciences and Technologies
25 - 29 October, Sakarya / Turkey
2019.itwccst.org

Effects of Ultrasonic-Treatment Temperature on $CoAl_2O_4$ Colour Performance

Fatma Tuğçe ŞENBERBER

Department of Civil Engineering, Nisantasi University, Istanbul, Turkey.

fatma.senberber@nisantasi.edu.tr; tsenberber@gmail.com

Keywords: Pigment, $CoAl_2O_4$, spinel, colour analysis, ultrasonic synthesis

ABSTRACT

Inorganic pigment of Co-Spinel was synthesized by ultrasonic assisted co-precipitation method at different ultrasonic-treatment temperatures. The effect of ultrasonic treatment on reaction mechanism is also detailed. The colour analyses results indicated that the lowest b* value of -41.31 was observed at the ultrasonic treatment of 50°C. The synthesized bright blue powders were identified as Cobalt Aluminate Oxide ($CoAl_2O_4$, powder diffraction file number of 00-044-0160) in X-Ray diffraction (XRD) analyses. The colour of synthesized compound was proved by adsorption peaks at the wavelengths of 550, 610 and 645 nm in UV-Vis spectroscopy (UV) results. The experimental results showed that spinels could be synthesized at higher crystallinity features by the use of ultrasonic treatment.

INTRODUCTION

Spinel type inorganic pigments are chemically and thermally stabile at high temperature. $CoAl_2O_4$ is a typical type of spinel and is also known as Thenard's blue. It is preferable especially in the coloration of ceramics, glass, plastics and porcelain enamels [1, 2].

The colour performance, crystallinity, particle shape and size of pigments are essential characteristic to determine their quality. These characteristics will affect their printing and applications. Recent printing technology is based on two main methods:

- Analog printing that includes the use of micro-structured inks
- Digital printing (ink-jet printing or 3D printing) that includes the use of nano-structured inks [3]

The traditional preparation methods of $CoAl_2O_4$ is based on the solid-state reaction of cobalt and aluminium sources at higher temperatures. With the developments in technology and science, hydrothermal methods have been began to use as previous step to increase the contact of raw materials particles before the calcination. Pechini, hydrothermal, polyol, solution combustion, co-precipitation are the common methods of $CoAl_2O_4$ synthesis [4-6]. The synthesis procedure includes the dissolution of cobalt and aluminium sources separately in an organic solvent or water medium at the pH values higher than 8. Capping agents, such as N, P, O or S terminated ligands, can be preferred to form the particle size and shape. Particle properties are notable for the pigments' colour performance and application. The researches indicated that pre-treatments play important role in the colour performance of synthesized pigment particles. In these experiments, it is aimed to prepare purple-pink solutions of proper complexes before the reaction. After the preparing the complexes including Co and Al at room temperatures, the reaction repeated at different temperature and times [1, 2, 4-6].

The ultrasonic beam can be used in synthesis procedures to obtain a homogenous interaction between the materials and to obtained proper and smaller particles [7]. This technique generally is preferred because of the increases in product formation and the decreases in the reaction times.

During the ultrasonic-treatment, there may be temperature increase in liquid medium when the ultrasonic beam contact with the particles. To use of ultrasonic beam in the synthesis procedure, it should be experimented the effects of this temperature effect on the product characteristics. Different temperatures were experimented during ultrasonic-treatment and the effects on characterization is compared.

EXPERIMENTS AND RESULTS

The cobalt source of $CoCl_2 \cdot 6H_2O$ and aluminium source of $AlCl_3 \cdot 6H_2O$ were used for the synthesis. $CoCl_2 \cdot 6H_2O$ was supplied from Alfa Aesar

with a minimum purity of 98%. $AlCl_3 \cdot 6H_2O$ (with a minimum purity of 98%) and NaOH were provided from Merck Chemicals.

Ultrasonic-assisted co-precipitation method was used fot the $CoAl_2O_4$ synthesis. Co and Al sources were dissolved in liquid medium at the stoichiometric ratio (Co/Al) of 0.5. The mixture pH adjusted to the 13 by using the 3M NaOH solution. Ultrasonic homogenizer of Bandelin Sonopuls (HD 2070 (20 kHz) model) was employed to precipitate the midproduct before the calcination. The temperatures were selected as 25, 50 and 75°C for the ultrasonic-treatment. The obtained pink-purple solutions were washed with water and filtered. The filtrates were dried at 105°C in EcoCELL 111 model oven; and calcined at 1200°C for 3 hours by using the high temperature furnace of Protherm MOS 180/4. The samples ultrasonic treated at 25, 50 and 75°C were coded as S-1, S-2 and S-3, respectively.

The intense blue particles were conducted to PCE CSM 1 model colorimeter for the colour analysis. For the identification of samples, PANalytical Xpert Pro X-Ray Diffractometer was used at the analyses conditions of 40mA, 45 kV and 2θ range of 7°–90°. Perkin Elmer UV-Vis spectropohotometer was preferred for the analyses of characteristic bands between the Co and Al atoms in the range of 500-700 nm. For the UV analyses the samples were dissolved in ethanol.

RESULTS AND DISCUSSION

In colour coordinate, the colour of a pigment can be expressed with three main parameters: L* is the lightness range from 0 (black) to 100 (white), a* is used for the range from – (green) to + (red) and b* is used the range from – (blue) to + (yellow). Chroma (c*) and Hue angle (h*) are the derived magnitudes of colour coordinate system. The c* value is the distance from the L* axis and begins at 0 in the centre. h* begins at the positive side of a* axis and is expressed in degrees.

The chromatic parameters of prepared cobalt aluminates are given in Table 1. The lowest b* value of sample prepared at the ultrasonic treatment temperature of 50°C indicates that the targeted reaction mechanism is achieved. According to the colour circle, the h* angle is also in good agreement with the blue colour.

Table 1. The chromatic parameters of samples

Sample Code	L*	a*	b*	c*	h*
S-1	32.40	-23.20	-12.10	26.16	207.55
S-2	34.09	9.61	-41.31	42.42	283.10
S-3	22.06	-2.07	-2.86	3.53	234.20

Images of synthesized pigments are presented in Figure 1. The obtained colour analyses results are consistent with the literature [8]. The synthesis mechanism of $CoAl_2O_4$ can be explained with an optical view. Co source turns the black particles of Co_3O_4 in the lack of Al source or other reaction parameters. Because of the use of constant Co/Al ratio in experiments, the factor effect on the reaction mechanism will be temperature of ultrasonic treatment. With the proceeding of reaction mechanism, the black particles form to the dark green Co_2AlO_4 and then bright blue $CoAl_2O_4$. In this sight, the spinel structure of $CoAl_2O_4$ is prepared in S-2.

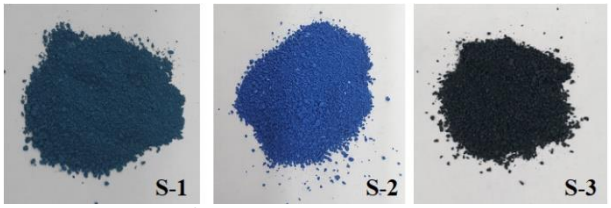

Figure 1. Images of synthesized pigments

XRD patterns of prepared cobalt aluminates are seen in Figure 2. The synthesized phase identified as Cobalt Aluminum Oxide with the powder diffraction file of "00-044-0160". Although the $CoAl_2O_4$ formation begins in XRD pattern of S-1, the presence of Co_2AlO_4 can be seen in sample images in Figure 1. Both the required characteristic peak formation XRD and bright blue image prove that the desired conversion is achieved in S-2. The increase in reaction temperature higher than 50°C affects the bonds in the Co and Al pre-complexes adversely. It might be explained with the transform of Co source to amorphous Co_3O_4, which can be understand with the black colour in S-3 image (Figure 1).

UV-Vis spectra of synthesized pigments can be seen in Figure 3. The adsorption peaks at the wavelengths of 550, 610 and 645 nm indicate the blue colour of synthesized compound. The observed band values are in good agreement with Gao et al. (2017) [9].

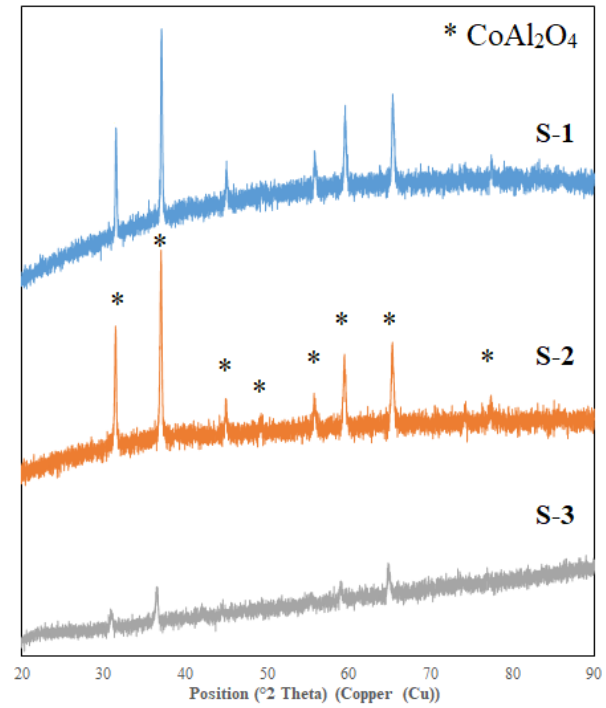

Figure 2. XRD patterns of synthesized pigments

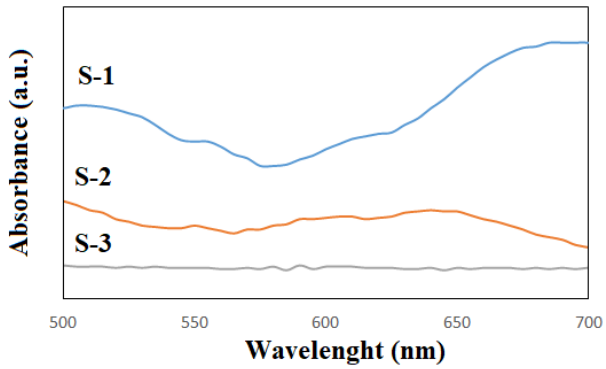

Figure 3. UV-Vis spectra of synthesized pigments

CONCLUSION

The spinel type of cobalt aluminate ($CoAl_2O_4$) is prepared with an ultrasonic assisted co-precipitation method. he effects of temperature of ultrasonic treatment on the chromatic features of synthesized pigments is experimented and characterized. For this purpose, $CoCl_2 \cdot 6H_2O$ and $AlCl_3 \cdot 6H_2O$ were reacted in liquid medium with the assistance of ultrasonic treatment at temperatures of 25, 50 and 75°C. After the obtained pink solutions were calcined at 1200°C, the intense blue particles were observed. The samples were characterized with the techniques of X-ray diffraction (XRD), UV spectroscopy and colour analysis. Experimental results indicated that ultrasonic treatment increased the colour performance of synthesized blue pigments. According to the characterization, the optimum reaction temperature is determined as 50°C.

REFERENCES

[1]Khademolhoseini, S.; Talebi, R. J. Mater. Sci.: Mater. Electron. **2016**, 27, 2938-2943.
[2]Zhang, A.; Mu, B.; Wang, X.; Wen, L.; Wang A. Front. Chem. **2018**, 6, 1-11.
[3]Rajan, K.; Roppolo, I.; Chiappone, A.; Bocchini, S.; Perrone, D.; Chiolerio, A. Nanotechnol. Sci. Appl. **2016**, 9, 1-13.
[4]Chang, Y.; Feng, T.; Wua, C.; Chen, Y.; Ke, K.; Liu, Y.; Wang, H.; Dong, S. Adv. Powder Technol. **2018**, 29, 1222–1229.
[5]Han, M.; Wang, Z.; Xu, Y.; Wu, R.; Jiao, S.; Chen, Y.; Feng, S. Mater. Chem. Phys. **2018**, 215, 251-258.
[6]Aguilar-Elguézabal, A.; Román-Aguirre, M.; De la Torre-Sáenz, L.; Pizá-Ruiz, P.; Bocanegra-Bernal, M. Ceram. Int. **2017**, 43, 15254-15257.
[7]Cains, P. W.; Martin, P. D.; Price, C. J. Org. Process Res. Dev. **1998**, 2, 34−48.
[8]Dippolito, V.; Andreozzi, G. B.; Bosi, F.; Halenius, U. Am. Min. **2012**, 97, 1828–1833.
9Gao, Y.; Chang, H.; Wu, Q.; Wang, H.; Pang, Y.; Liu; F.; Zhu, H.; Yun, Y. Trans. Nonferrous Met. Soc. China. **2017**, 27, 863−867.

ITWCCST 2019
5th International Turkic World Conference on Chemical Sciences and Technologies
25 - 29 October, Sakarya / Turkey
2019.itwccst.org

The Inhibition Effect of Some Active Compounds from the Medical Plants on Breast Cancer

Faik GÖKALP*

**Kırıkkale University,Education Faculty, Department Of Mathematics and Science Education, Science Education Division, Yahşihan/Kırıkkale, 71450 Turkey*

akgokalp@gmail.com

Keywords: Piperine, Carvacrol, Capsaicin, Cucurbitacin E, Cucurbitacin I,breast cancer, docking

INTRODUCTION

The spices obtained from traditional medicinal plants have been in use in kitchen and medical preparations for a long time. The active substances derived from medicinal plants are mainly used for their pharmacological and biological activities, including in vitro or in vivo studies. Black pepper, known as the King of Spices, is the most important and most consumed spice in the world and is an indispensable ingredient in food processing due to its exquisite flavor and health benefits. Piperine, the most abundant alkaloid of pepper, was isolated from the pepper extract as a yellow crystalline compound (1). Piperine obtained from black pepper prevented the growth of cell cancer by inhibiting cell cycle progression (2). Carvacrol is the main ingredient in essential oils of thyme species. Capsaicin is a compound found in hot peppers and triggers cell cycle arrest by modulating the epithelial growth factor receptor / HER2 pathway and p27 expression in estrogen receptor positive and negative cells (3). Carvacrol (4), Capsaicin (5), Cucurbitacin E (6) and Cucurbitacin I (7) active substances had an inhibitory effect on breast cancer cells. Cucurbitacins exhibited potent anti-proliferative activities against breast cell lines; among them, cucurbitacin E showed the same cytotoxicity as colchicine, which may be recommended as potential applications on cancer treatment (8). The effects of the aforementioned active compounds for breast cancer from medicinal plants were investigated using docking (9). Comparison results were calculated to determine the most active substance for the inhibition of breast cancer.

MATERIALS AND METHODS

In this study, the inhibitory effect of Piperin, Carvacrol, Capsaicin Cucurbitacin E and I, one of the important active substances obtained from medicinal plants, on breast cancer was compared using docking (9). It was put forward what kind of interactions could occur. These theoretical studies are very important in terms of guiding the experimental studies and preventing the loss of time and substances.

RESULTS AND DISCUSSION

The attractiveness of natural compounds as medicines is partly due to their potential to affect many components in the carcinogenic pathway. This study focuses on key molecular targets that play a role in cancer progression and differentiation. The docking results of the traditionally used medicinally important active compounds on the inhibitory effect of breast cancer PI3K receptors (10) are given in Table 1.

Docking results related to the inhibitory effect of important active compounds on conventionally used medicinal plants on breast cancer receptors are given in Table 1.

Table 1. The inhibition effect of important active compounds in traditionally used medicinal plants on breast cancer

Active compounds/ breast cancer	E free binding energy score (kcal/mol)	Inhibition constant (Ki)	H-binding energy (kcal/mol)	Elctrostatic energy (kcal/mol)	Internal energy (kcal/mol)
Carvacrol	-5.20	155.15 uM	-5.73	-0.07	-5.80
Piperine	-6.84	9.69 uM	-7.67	-0.05	-7.72
Capsaicin	-4.68	372.89 uM	-6.80	-0.15	-6.96
Cucurbitacine E	-6.18	29.75 uM	-7.89	-0.16	-8.05
Cucurbitacine I	-6.56	15.52 uM	-7.28	-1.39	-8.67

The interaction of Piperin, an important active ingredient in black peper traditionally used medicinal plants, with the breast cancer receptor is given in Figure 1.

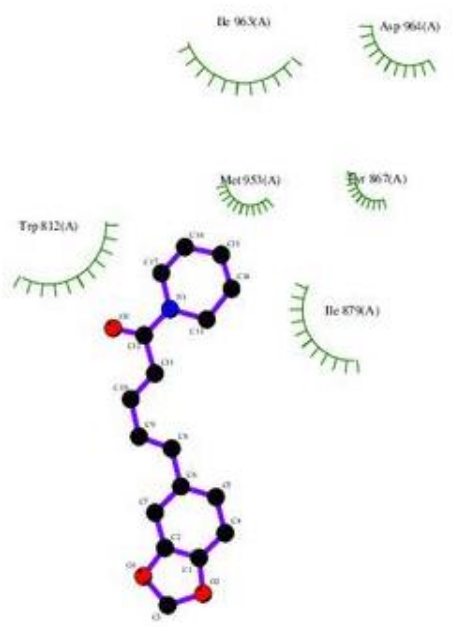

Figure 1. The interaction of Piperin with the breast cancer receptor

The interaction and interaction of Piperin with the breast cancer receptor is summarized in Table 2.

Table 2. The interaction of Piperine with breast cancer receptor

hydrophobic	other
ILE963 (-1.1165)	ASP964 (-0.5836)
TRP812 (-1.0686)	
ILE879 (-0.871)	
MET953 (-0.235)	
TYR867 (-0.1688)	

The interaction of Cucurbitacine I with the liver cancer receptor is given in Figure 2.

CONCLUSION

According to the results of the theoretical chemical calculations, the inhibitory effect of Piperin on PI3K receptor of breast cancer is quite high and it is understood that this interaction is hydrophobic. In conclusion, the effect of Piper on breast cancer can be investigated by supporting experimental studies.

ACKNOWLEDGEMENTS

This study is supported by the Scientific Research Projects of Kırıkkale University (BAP-2017/019,2018/033).

REFERENCES

1. Gorgani, L., Mohammadi, M., Najafpour, G. D. ve Nikzad, MPiperin-Black Pepper Bioactive Compound: From Insulation to Medical Formulations. Comprehensive Comments on Food Science and Food Safety, **2017**,16: 124-140.
2. Yichun Zou, Pian Gong, Wenyuan Zhao, Jianjian Zhang, Xiaolin Wu, Xin Xin, Zhongwei Xiong, Zhengwei Li, Xiaohui Wu, Qi Wan, Xiang Li, Jincao Chen, Quantitative iTRAQ-based proteomic analysis of Piperin-protected cerebral ischemia / reperfusion injury in rat brain, Neurochemistry International, **2019**, 124,51-61.
3. Fattori, V., Miriam SN Hohmann, Ana C. Rossaneis, Felipe A. Pinho-Ribeiro ve Waldiceu A. Verri Jr., Capsaicin: Defining Mechanisms and Therapy of Pain and Other Pre-Clinical and Clinical Uses, Molecula, **2016**, 21, 844.
4. Arunasree, K.M., Anti-proliferative effects of Carvacrol on human metastatic breast cancer cell line, MDA-MB 231. Phytomedicine, **2010** 17, 581-588.
5. Lozano C, Córdova C, Marchant I, et al. Intracellular aggregated TRPV1 is associated with lower survival in breast cancer patients. Breast Cancer (Dove Med Press). **2018**;10:161–168.
6. Zhang, TJ Li, Y. Dong, D. Zhai, L. Lai, F. Dai, H. Deng, Y. Chen, M. Liu, Z. Yi, , Cucurbitacin E inhibits breast tumor metastasis by suppressing cell migration and invasion Breast Cancer Res. Treat., **2012** 135, 445-458.
7. Karakuş, F., Yılmaz, K., Eyol, E., & Ünüvar, S., Combination of 2 Bioactive Compounds in the Treatment of Breast Cancer: Triterpenoid Cukurbitacin I and Phenolic CAPE. Natural Product Communication **2019**.
8. Wang, X., Mine Tanaka, Herbenya Silva Peixoto ve Michael Wink, Cukurbitacins: Explaining their interaction with the cell skeleton. PeerJ., **2017** 5: e3357.
9. Bikadi, Z., Hazai, E., PM6 yarı-ampirik yönteminin proteinlerin modellenmesine uygulanması, AutoDock J. Cheminf. **2009** 1, 15.
10. Qin H, Liu L, Sun S, et al. The impact of PI3K inhibitors on breast cancer cell and its tumor microenvironment. PeerJ. **2018**;6:e5092.

ITWCCST 2019
5th International Turkic World Conference on Chemical Sciences and Technologies
25 - 29 October, Sakarya / Turkey
2019.itwccst.org

The Inhibition Effect of Some Active Compounds from the Medical Plants on Liver Cancer

Faik GÖKALP*

**Kırıkkale University,Education Faculty, Department Of Mathematics and Science Education, Science Education Division, Yahşihan/Kırıkkale, 71450 Turkey*

akgokalp@gmail.com

Keywords: Carvacrol, Piperine, Capsaicin, Cucurbitacins, Liver cancer, docking

INTRODUCTION

Medicinal plants have been used for the treatment of various diseases. Major modern drugs are produced directly or indirectly from medicinal plants. The components of the medicinal plant may interact with each other, and this interaction may be beneficial to or against both, or may counteract their deleterious effects. The plant-derived compounds can significantly improve difficult-to-treat diseases such as cancer. Many plant materials, in particular active compounds from their extraction, are tested for pharmaceutical purposes. One of them is Carvacrol (2-methyl-5- (1-methylethyl) - phenol). It is a monoterpenic phenol which is isomeric with thymol found in many aromatic plants, including origanum species. Carvacrol has anticarcinogenic and antiproliferative properties, which have been shown to inhibit HepG2 cell growth by inducing apoptosis by caspase-3 activation, reducing PARP separation and reduced Bcl-2 gene expression . Carvacrol has been reported to have antiproliferative effect in liver cancer cells (1). Piperin (2), Capsaicin (3), Several cucurbitacin including Cucurbitacin E, I have been shown to have antiproliferative and anticancer activities (4). In this study, the inhibitory effects of the above-mentioned active compounds from medical plants in liver cancer were examined using docking (5). The comparison results were calculated to detect the most active substance for the inhibition of liver cancer. The global tendency of synthetic compounds is directed to herbal medicines, which we can call return to nature to prevent diseases. Many medicinal plants obtained from nature are used as a source of healing (6).

MATERIALS AND METHODS

In this study, the inhibitory effect of Piperin, Carvacrol, Capsaicin Cucurbitacin E and I, the important active substances obtained from medicinal plants, was compared using docking (5). It was put forward what kind of interactions could occur. These theoretical studies are very important in terms of guiding the experimental studies and preventing the loss of time and substances.

RESULTS AND DISCUSSION

The attractiveness of natural compounds as medicines is partly due to their potential to affect many components in the carcinogenic pathway. This study focuses on key molecular targets that play a role in cancer progression and differentiation. liver cancer receptors have been identified as PDB ID: 3S35 (7).

The docking results related to the inhibitory effect of important active compounds on the liver receptors of conventionally used medicinal plants are given in Table 1.

Table 1. The **i**nhibition effect of important active compounds on traditionally used medicinal plants on liver cancer

Active compounds/ Liver cancer) (3s35))	E free binding energy score (kcal/mol)	İnhibition constant (Ki)	H-binding energy (kcal/mol)	Elctrostatic energy (kcal/mol)	Internal energy (kcal/mol)
Carvacrol	-3.70	1.94 mM	-4.14	-0.15	-4.30
Piperine	-4.48	524.29 uM	-5.32	-0.03	-5.35
Capsaicin	-3.84	1.54 mM	-6.05	-0.13	-6.18
Cucurbitacine E	-5.00	215.94 uM	-6.47	-0.33	-6.80
Cucurbitacine I	-5.53	87.67 uM	-6.67	-0.04	-6.71

The interaction of Cucurbitacine I with its liver cancer receptor, an important active ingredient in traditionally used medicinal plants, is given in Figure 1.

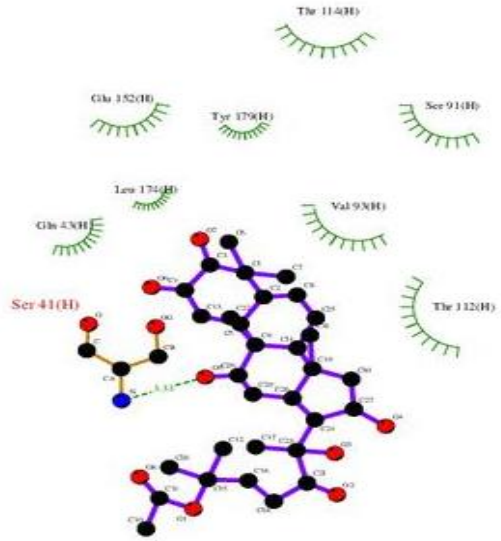

Figure 1. The interaction of Cucurbitacine I with liver cancer receptor

The interaction of cucurbitacine I with liver cancer receptor and the regions it interacts with is summarized in Table 2.

Table 2. The interaction of Cucurbitacine I with liver cancer receptor

hydrogen bonds	polar	hydrophobic	other
TYR179 (-0.394)	GLU152 (0.0611)	LEU174 (-0.4717)	SER41 (-17.180)
THR114 (-0.174)	SER91 (1.1746)	VAL93 (1.631)	

The interaction of Cucurbitacine E with its liver cancer receptor is given in Figure 2.

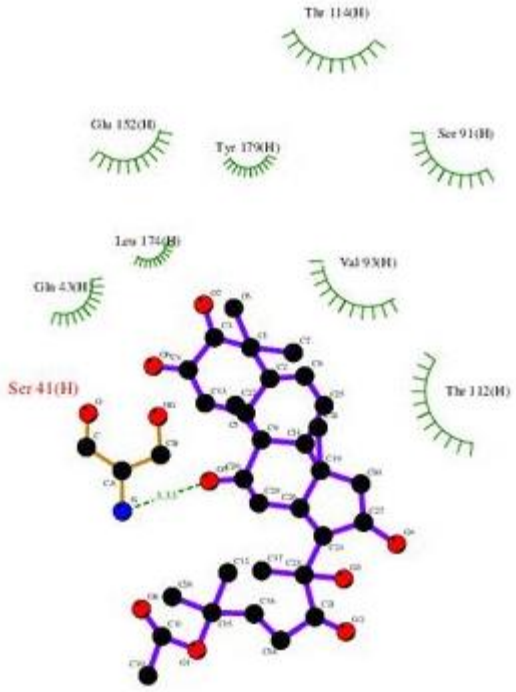

Figure 2. The interaction of Cucurbitacine E with liver cancer receptor

The interaction of Piperine, an important active ingredient of the black cumin, with the liver cancer receptor is given in Figure 3.

Figure 3. The interaction of Cucurbitacine I with liver cancer receptor

CONCLUSION

According to the results of the theoretical chemical calculations, the inhibitory effect of Cucurbitacine E and I on liver cancer receptors seems to be quite high, especially for Cucurbitacine I, we can state that this value is higher and that the interaction occurs as hydrogen bond formation. In conclusion, Cucurbitacine E and I can be supported by experimental studies to investigate its effect on liver cancer.

ACKNOWLEDGEMENTS

This study is supported by the Scientific Research Projects of Kırıkkale University (BAP-2017/019,2018/033).

REFERENCES

1. Yin, QH, Yan, FX, Zu, XY, Wu, YH, Wu, XP, Liao, MC, Deng, SW, Yin, LL ve Zhuang, YZ, Anti-proliferative and pro-apoptotic effect of carvacrol human hepatocellular carcinoma cell line HepG-2. the Sitoteknoloj **2012** 64: 43-51.

2. Tawani A, Amanullah A, Mishra A, Kumar A. İnsan G-kuadrupleks DNA sekanslarını hedef alarak Piperinin kanseri önleyen kanıtları. Sci Rep. **2016**; 6: 39239.

3. Zhong, Faqiang, Liu, Zhiguang, Han, Yujie, Guo, Yujing, Electrochemical Sensor for Precise Detection of Capsaicin Using Pd Decorated Graphene Oxide, Electroanalysis, **2019** 31-6, 1182 - 1188.

4. Alsayari, Abdulrhman, - Halaweish, Fathi, - Gurusamy, Narasimman, The role of salad water in the fight against cucumbers: A mechanical examination, Evaluation of Pharmacognosy, Phcog Rev., **2018** 12-24,157-165.

5. Bikadi, Z., Hazai, E., Application of PM6 semi-empirical method to the modeling of proteins,AutoDock J. Cheminf. **2009** 1, 15.

6. Fabricant, D.S, Farnsworth N.R., Discovery of drugs used in traditional medicine, Environmental Health Perspective.**2001**; 109 1: 69-75.

7. M.P.Santhi, G.Bupesh, V.Senthil, Kumar,, K.Meenakumari,, K.Prabhu,, S.Sugunthan,E.Manikandan, K.Saravanan, Anticancer Activity And Drug Likeliness Of Quinoline Through Insilico Docking Against Cervical And Liver Cancer Receptors, Indian Journal of Medical Research and Pharmaceutical Sciences, **2016**; 3(9).

ITWCCST 2019
5th International Turkic World Conference on Chemical Sciences and Technologies
25 - 29 October, Sakarya / Turkey
2019.itwccst.org

3(2*H*)-Pyridazinones: Synthesis as Antifungal Agents, *in silico* Fungal CYP51 Inhibition

Yaren Nur ZENNİ[1], Zeynep ÖZDEMİR[2], Burak KUZU[3], İsmet KUTLUK[4]

[1]*İnönü University Faculty of Pharmacy, Malatya, Turkey*

[2]*Department of Pharmaceutical Chemistry, İnönü University Faculty of Pharmacy, Malatya, Turkey*

[3]*Department of Pharmaceutical Chemistry, Yüzüncüyıl University Faculty of Pharmacy, Van, Turkey*

[4]*Department of Pharmaceutical Microbiology, Gazi University Faculty of Pharmacy, Ankara, Turkey*

zeynep.bulut@inönü.edu.tr

Keywords: Pyridazinone, antifungal, CYP51 enzyme

,

INTRODUCTION

The studies carried out to develop potent and effective antifungal compounds are significant not only for the control of the severe infections but also for the prevention and the treatment of the possible infections caused by the cancer, surgical processes and other treatments. On the other hand, fungal infections increase on the cases which surpass immune system such as tuberculosis, cancer, AIDS and transplantation and could be a reason for death. It is, therefore, crucial that compounds whose influential spectrum is extensive and side effects are lowered to the minimum be developed[1-3]. Among the pharmacophore groups responsible for the antifungal activity, pyridazinone ring is the important ones used during the synthesis of the more effective and extensive spectrum anti-microbials. Pyridazinone derives have been also defined as heterocyclic compounds that have significant biological effects such as anti-inflammatory, antipyretic, antiviral, anti-tumoral, potential HIV-1 inhibitor, and antidepressant, so we have been synthesized some 3(2*H*)-pyridazinone derivative as antifungal compounds. chemical structure of compounds was confirmed by H^1-NMR and mass spectral data[4-8]. Molecular modeling studies have been carried out to predict the mechanism of action of antifungal activity because of the moderate antifungal activity of the compounds. Molecular modeling studies have screened whether compounds inhibit the CYP51 enzyme of *Candida albicans*[9].

Candida albicans is the major pathogen identified in systemic candidiasis. *C. krusei* is multidrug resistant and less susceptible to fluconazole. Azole antifungals are known to inhibit fungal CYP51 through coordination with heme iron via their azole N in the catalytic domain, however several non-azole inhibitors have so far been introduced[10-12]. Herein we provide mechanist insights into *in silico* inhibition of fungal CYP51 by some 3(2*H*)-pyridazinone derivatives reported to have moderate antifungal activities and show the importance coordination with heme iron in the catalytic domain of fungal CYPs.

MATERIALS AND METHODS

A series of 6-substituted-3(2*H*)-pyridazinone derivatives (Figure 1) were designed, synthesized, and their antifungal effects on *C. albicans* and *C. krusei* were evaluated. We obtained our compounds by the reaction of various benzaldehydes, isocyanates and isothiocyanates with 6-substituted-3(2*H*)-pyridazinone-2-yl propiohydrazide and determined their antifungal activities by using microdilution method. The structures of these pyridazinone derivatives were confirmed by their ^{1}H-NMR spectra and elementary analysis.

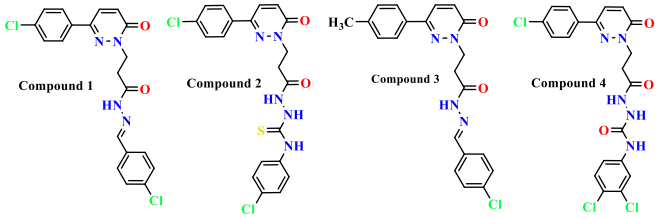

Figure 1. Structures of compounds (4a-d).

RESULTS AND DISCUSSION

The structures and antifungal activity results of 3(2*H*)-pyridazinone derivatives were shown in Table 1.

Table 1. MIC* values (µg/mL) of compounds against *C. albicans* and *C. krusei.*

Compound	*C. albicans*	*C. krusei*

1	128	128
2	128	512
3	128	128
4	64	128
Ketoconazole	2	2
Fluconazole	2	64

* Minimum inhibitor concentration (µg/mL)

Drawing of synthesized compounds and 3D optimizations were done by Gaussian 09 package program. Optimization method was made as Semi-empirical PM6 Charge: 0, Spin: singlet, solvation: none. The resulting optimization output files are saved as pdb extension files. The protein molecule was obtained from the protein data bank Structure of CYP51 from the pathogen Candida glabrata (PDB code: 5JLC). The macromolecule was reconstructed with the discovery of the ligand molecules and water molecule by the Discovery studio 2016 program. Again with the same program, the amino acids in the active region were determined. Enzyme and ligand molecules were prepared and a grid map was prepared by Autodock 4.2 program.

The search grid of 5JLC was identified as center_x: -38.584, center_y: 75.808, and center_z: -23.4 with dimension size_x: 70, size_y: 70, and size_z: 70. The docking parameters are set to default and the population size is set to 300 and docking is done. The enzyme ligand conformation of the conformation of the smallest binding energy from 10 different conformation was created for each molecule obtained. Then, this complex was studied with the Biovia Discovery Studio for determining of the 2D diagram of the interaction with amino acids in the ligand binding region (Figure 2).

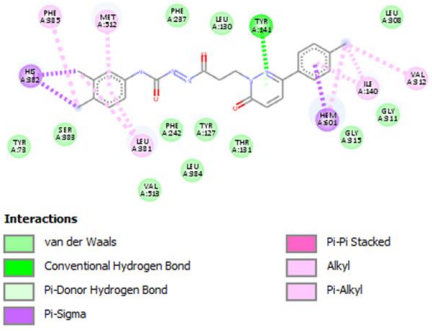

Figure 2. Binding modes of **4** in CGCYP51 catalytic domain.

When all molecules are examined, they all interact with HEM601 and amino acids in the active site. When the docking results of the designed molecules are examined, it can be seen that the molecule **4** binds to the active region of the enzyme with higher affinity (Table 2).

Molecule 5 interacts with the HEM601 group in the active site of the enzyme as pi-pi shape. In addition, chlorine atoms in the designed molecule interacted with the amino acids responsible for the active site and showed higher affinity binding (Figure 2). By adding chlorine atoms to the structure, it can be concluded that more effective molecules could be designed. In addition, it is highly desirable for all molecules to exhibit activity at the nM level, in particular to give the molecule **4** a theoretical inhibition constant of 5.99 nM (Table 2).

Table 2. Molecular docking binding scores and binding interactions of **4a-f** and selegiline within the CGCYP51 active site.

Molecule	Binding Energy (kcal/mol)	Inhib. Constant (nM)
1	-11.03	8.21
2	-10.99	8.86
3	-10.66	15.44
4	-11.22	5.99

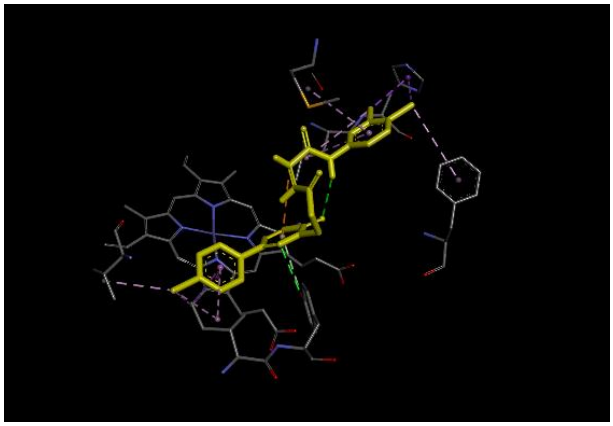

Figure 3. Binding modes of **4** in CGCYP51 catalytic domain.

CONCLUSION

Glide predicted a good fit for **1-4** in the lipophilic active gorge of CGCYP51 making various hydrophobic interactions, similarities to the co-crystallized itraconazole. Glide scores of **1-4** were relatively high, higher than fluconazole, but still lower than itraconazole possibly due to lacking an azole group to coordinate with the iron of heme group. 3(2*H*)-pyridazinone derivatives probably show their antifungal activities through fungal CYP51 inhibition.

REFERENCES

[1] Binder U., Lass-Floerl C., Medit. J. Hemat. Infect. Dis.,2011, 3(1), e20110016.
[2]Silva S., Negri M., Henriques M., Oliveira R., Williams D.W., Azeredo J., FEMS Microbiol. Rev., 2012, 36(2) 288-305.

[3]Pfaller M.A., Castanheira M., Lockhart S.R., Ahlquist A.M., Messer S.A., Jones R.N., J. Clin. Microbiol.,2012, 50(4), 1199-1203.
[4]Asif M., Cent. Eur. J. Exp. Biol., 2017, 5(1), 1-19.
[5]Asif M., Mong. J. Chem., 2016, 17(43), 28-33.
[6]Singh J, Sharma D, Bansal R. J Heterocycl Chem 2017;54(5):2935-2945.
[7]El Rayes SM, Ali IAI, Fathalla W., J. Heterocycl. Chem., 2019, 56, 51-59.
[8]Akhtar W, Shaquiquzzaman M, Akhter M, Verma G, Khan MF, Alam MM., Eur. J. Med. Chem., 2016, 123, 256-281.
[9]Odds F.C., Brown A.J., Gow N.A., Trends Microbiol., 2003, 11(6), 272-279.
[10]Balding P.R., Porro C.S., McLean K.J., Sutcliffe M.J., Marechal J.D., Munro A.W., de Visser S.P., J. Phys. Chem. A. 2008, 112(50), 12911-12918.
[11]Vermitsky J.P., Edlind T.D., Agents Chemother. 2004, 48(10), 3773-3781.
[12]Lamb D.C., Kelly D.E., SchunckW.H., Shyadehi A.Z., Akhtar M., Lowe D.J., Baldwin B.C., Kelly S.L., J. Biol. Chem. 1997, 272(9) 5682-5688.

ITWCCST 2019
5th International Turkic World Conference on Chemical Sciences and Technologies
25 - 29 October, Sakarya / Turkey
2019.itwccst.org

Effect of Polyethylene Glycol 600 on Polymeric Membrane Morphology

Yasemin Yildiz*, Aynur Manzak
*Vocational School of Health Services,Department of Medical Services and Techniques, Sakarya University, TR-54100, Sakarya, Turkey
Department of Chemistry, Faculty of Art and Science, Sakarya University, TR-54187, Sakarya, Turkey
yyildiz@sakarya.edu.tr

Keywords: Polyethylene glycol, Adsorption, Polymeric membrane

INTRODUCTION

Most of the environmental problems are caused by heavy metals. This problem increases the need to develop new methods for today's treatment plants to be more effective and clean. Polymeric membranes are a method that can meet this need. Polymeric membranes consist of a polymer solution obtained by dissolving a polymer in a suitable solvent and a carrier capable of selectively separating the desired metal or contaminants. Polymer inclusion membranes often provide an alternative to conventional solvent extraction in which excessive amounts of highly volatile and easily flammable solvents are used (Saf 2010, 23). To date, many interesting studies have been done on polymer inclusion membranes. Recently, the factors affecting the morphology of the membrane in these studies also come to the fore. Among these factors, the use of various modifiers, as well as the use of pore-forming substances, is noteworthy. Increasing the efficiency of a membrane with the desired porosity is the greatest desire of researchers worldwide (Roy et al.2017, 5708– 25).

Polyethylene glycol (PEG), alcohols, glycerol, and polyvinylpyrrolidone (PVP) are used as inorganic and organic additives in membranes. These materials can be used as pore-forming agents. So, they improve membrane hydrophilicity along with pore interconnectivity. In this case, it contributes to the development of the membrane. In addition to these properties of additives, interactions between polymer and additives may affect the structure and properties of membranes. Pore formation can be obtained by adding polyethylene glycol in polymeric membranes. PEG is a linear polyether compound available in a variety of molecular weights. PEG is water-soluble. Polymer molecules are soluble by PEG. So, the solvency of the solvent can reduce by adding PEG. Therefore, the polymer chains tend to be in a more tense structure. As a result, the polymer chains would tend to be in a less expanded structure. Hydroxyl groups of polyethylene glycol can generate hydrogen bonding with the polymer in the membrane. That is, the role of PEG is connection polymer molecules with hydrogen bonding. So, the PEG may be called as cross-linkers. As a result, the apparent molecular size of the polymer grows, as seen from the SEM images. The type of polymer plays a vital role in the interaction with PEG. The effect of PEG on polymer was studied by Yingnan Feng et al. The presence of PEG increases the viscosity of polymer solutions. They found that polymer solutions became slightly more elastic with the addition of PEG (Yingnan Feng et al., 2017, 27-35).

Polyethylene glycol (PEG) was employed as an additive into polyvinyl chloride and cellulose triacetate in this work, and we investigated its effects on membrane formation and adsorption of the membrane.

Our study aimed to demonstrate the effect of adding polyethylene glycol on the membrane. It seemed that the SEM surface and cross-section images of the membrane varies with adding PEG.

Both before of adsorption and after of adsorption were investigated to illustrate the interactions between polymer and PEG and the effect of PEG on the resultant membranes, including morphology and pore structure. This study may contribute implications development of membranes that using PEG.

Experimental

All chemicals used are of analytical purity. Cellulose triacetate (CTA), Polyvinyl chloride (PVC), 2-nitrophenyl pentyl ether (2-NPPE), polyethylene glycol 600 (PEG 600) were obtained from Fluka, $CoCl_2.6H_2O$, $NiCl_2.6H_2O$, $3CdSO_4.8H_2O$, $CuSO_4.5H_2O$, and dichloromethane were purchased, Merck. All stock solutions were obtained by dissolving cobalt, copper, cadmium, and nickel salts in distilled water. Determination of surface characterization of membranes; FTIR Spectrophotometer with ATR technique (Perkim Elmer Spectrum Two Ir) and contact angle (Dataphysics) and Scanning Electron Microscope (SEM) was used. Membranes were placed in a solution containing cobalt, copper, cadmium, and nickel metals.

Preparation of Polymer Inclusion Membrane

Membrane was prepared by the pouring method. At room temperature, CTA or PVC (480 mg) was dissolved in 70 mL of dichloromethane or tetrahydrofuran. In the next step, 0.2 mL of 2-NPPE is added. PEG 600, and dichloromethane or tetrahydrofuran are added the solution was mixed, which was followed by 5 h of mixing to obtain a homogeneous solution. A glass square container (24 cm × 24 cm) was used and maintained at room temperature overnight to evaporate the solvent of the solution slowly. The solvent is evaporated off and washed with cold distilled water. The membrane is then removed from the container.

RESULTS AND DISCUSSION

It was possible to adsorb one or more components (metal ions, organic substances, etc.) by preparing different membrane compositions (different polymers, additives, etc.). Adsorption of cobalt, copper, cadmium, and nickel with polymer inclusion membranes from aqueous solutions was investigated. Both before of adsorption and after of adsorption were investigated to illustrate the interactions between polymer and PEG and the effect of PEG on the resultant membranes, including morphology and pore structure.

Determination of surface characterization of membranes; FTIR Spectrophotometer with ATR technique (Perkim Elmer Spectrum Two Ir) and contact angle (Dataphysics) and Scanning Electron Microscope (SEM) was used. The interactions between polymer and PEG and the effect of PEG on the resultant membranes, including morphology and pore structure, are shown in Table 1. Cross-section SEM images of membrane are shown in Table 2. The membrane changes from a void structure to a finger-like void structure with PEG adding in including polyvinyl chloride polymeric membrane (Table 1). This is not the case with cellulose triacetate in the membrane, such as polyvinylchloride. This is thought to be due to the difference in the molecular structure of the polymers. Cellulose triacetate has a more branched structure than polyvinyl chloride. Distinguishing characteristics of cellulose triacetate is that at least 92 percent of the hydroxyl groups are acetylated. When the surface of the membrane obtained after 7 hours is examined with SEM, the metals retained on the surface are shown in Table 3. Before and after adsorption, the image of the membrane surface is shown in Table 3. It is also understood that metals are retained on the membrane.

Table1. SEM images of membrane (Surface)

Consist of membrane	SEM images of membrane
PVC Tetrahydrofuran 2-NPPE	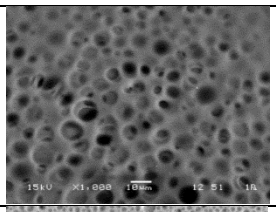
PVC PEG 600 Tetrahydrofuran 2-NPPE	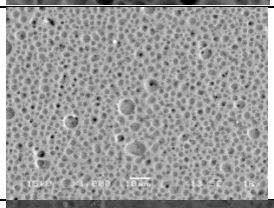
CTA Dichloromethane 2-NPPE	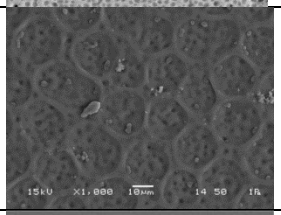
CTA Dichloromethane PEG 600 2-NPPE	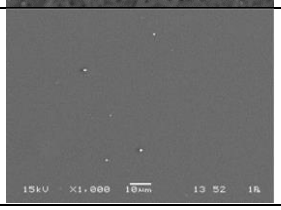

Table 2. Cross-section SEM images of membrane

Consist of membrane	Cross-section SEM images of membrane
PVC Tetrahydrofuran 2-NPPE	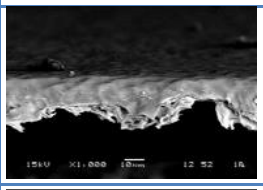
PVC Tetrahydrofuran PEG 600 2-NPPE	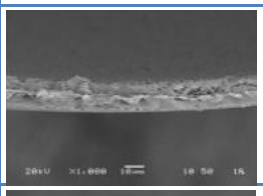
CTA Dichloromethane 2-NPPE	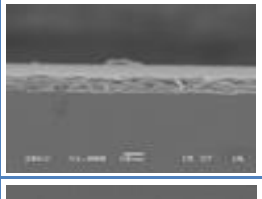
CTA Dichloromethane PEG 600 2-NPPE	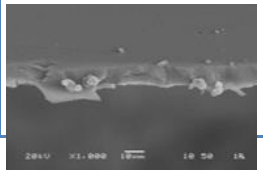

Table 3. The content of membranes and SEM image of membrane before and after experimental

Consist of membrane	SEM image of membrane	
	Before experimental	After experimental
CTA Dichloromethane PEG 600 2-NPPE	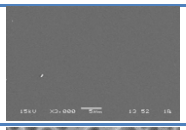	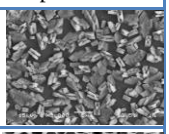
PVC Tetrahydrofuran PEG 600 2-NPPE	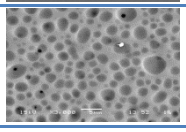	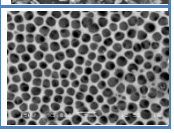

Membrane images after the experiment show the metals attached to the membrane surface. This is also supported by SEM-EDS analysis. (Figure 1-2). (Arous et al. 2010) stated in studies that the morphologies of the CTA membrane (view of surface) show that these membranes constituted by polymeric cellulose triacetate present a porous structure. Also, (Arous et al. 2010) found that the (CTA + plasticizer + carrier) membrane presents a dense structure where the pores of membrane have been filled by the carrier and plasticizer molecules yielding to the thick and less porous membrane.

In our study, the use of plasticization in the preparation of our membranes in the CTA membrane is shown in Table 2, where the pores are filled by plasticizing molecules. It explains why the pores in polyvinyl chloride are higher than cellulose tri-acetate because the polymer has strong C-Cl bonds, makes PVC suitable for mixtures, and is more prone to hydrogen bonding.

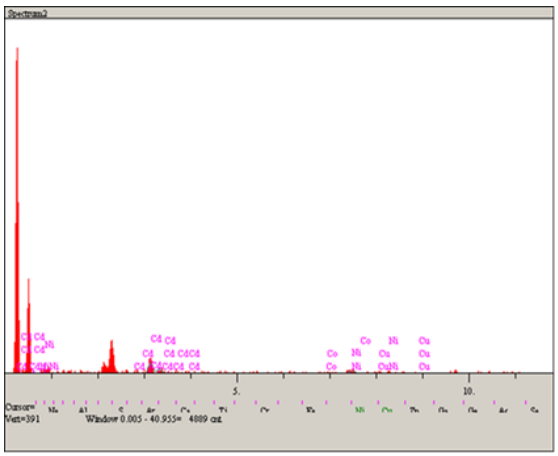

Elt.	Line	Intensity (c/s)	Error 2-sig	Conc	Units	
Co	Ka	1.43	0.755	4.949	wt.%	
Ni	Ka	5.67	1.506	22.240	wt.%	
Cu	Ka	2.30	0.959	11.216	wt.%	
Cd	La	15.10	2.457	61.595	wt.%	
				100.000	wt.%	Total

Figure 1. CTA, Dichloromethane, PEG 600, 2-NPPE

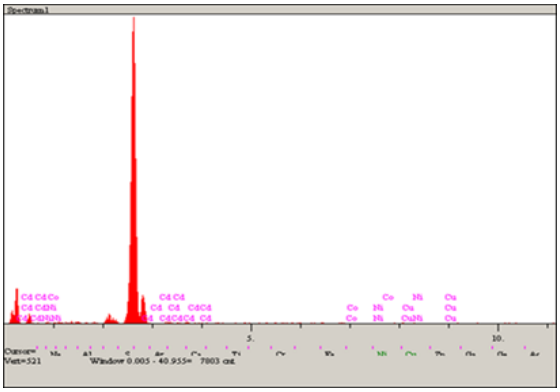

Elt.	Line	Intensity (c/s)	Error 2-sig	Conc	Units	
Co	Ka	1.22	0.699	21.051	wt.%	
Ni	Ka	0.61	0.494	13.868	wt.%	
Cu	Ka	1.54	0.784	49.209	wt.%	
Cd	La	1.08	0.658	15.873	wt.%	
				100.000	wt.%	Total

Figure 2. PVC, Tetrahydrofuran, PEG 600, 2-NPPE

The band observed in the spectra at 3350 cm^{-1} belongs to the O-H tensile vibration with hydrogen bonding. Furthermore, the bands at 1380 cm^{-1} and 1480 cm^{-1} in the spectrum, the band C-H bending at 2900 cm^{-1}, and the bands at 1180 cm^{-1} and 1120 cm^{-1} are the C-O stretching and O-H bending bands (Figure 3-4).

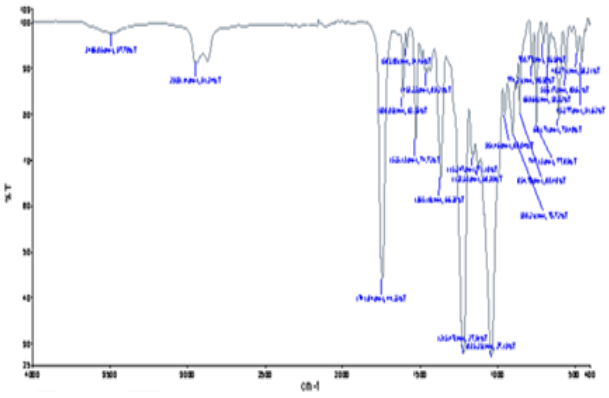

Figure 3. CTA, Dichloromethane, PEG 600, 2-NPPE

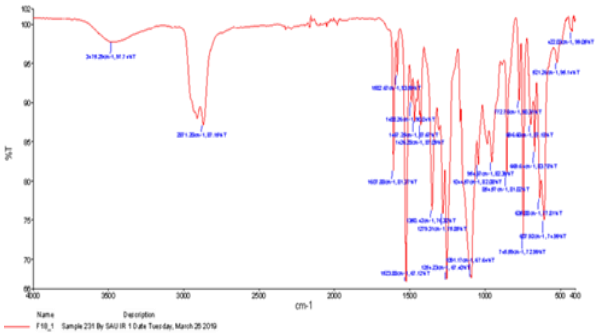

Figure 4. PVC, Tetrahydrofuran, PEG 600, 2-NPPE

Hydrophilic and hydrophobic characteristics of a polymer membrane was determined by measuring the contact angle. To measure the time dependence of the contact angle values 5µL of droplet volume was used. The contact angle was measured immediately after the dropping and at intervals of 10 seconds. The contact angle of CTA-dichloromethane-PEG 600-2-NPPE was measured as 57.2. The contact angle of PVC –PEG 600-tetrahydrofuran-2-NPPE was measured as 62,4.

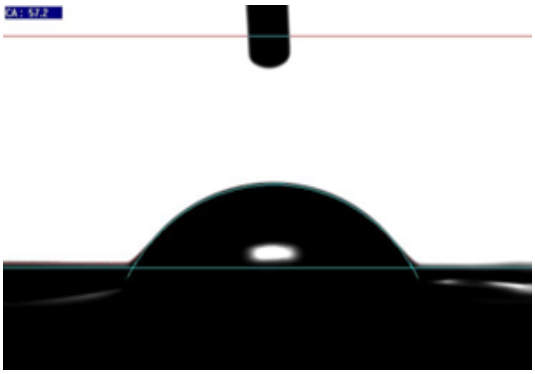

Figure 5. CTA, Dichloromethane, PEG 600, 2-NPPE

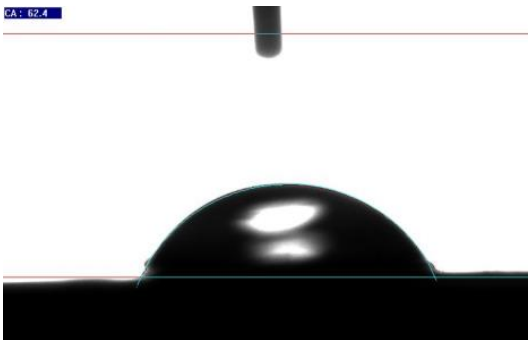

Figure 6. PVC, PEG 600,Tetrahydrofuran, 2-NPPE

CONCLUSION

Pore formation could be obtained by adding polyethylene glycol in polymeric membranes in our study, and the pores are filled by metal ions.

ACKNOWLEDGEMENTS

The authors, thanks to Prof. Dr. Akın Akıncı for his support. The equipment support of this work was provided by the Metallurgical and Materials Engineering of Sakarya University.

REFERENCES

[1]Arous O., Saad Saoud F., Kerdjoudj, H. IOP Conf. Series: Materials Science and Engineering **2010**, 12. doi:10.1088/1757-899X/12/1/012001
[2]Feng, Y., Han, G., Chung, T.S., Weber, M., Widjojo, N., Maletzko, C. Journal of Membrane Science, **2017,** 531, 27-35.
[3]Roy, K.J., Anjali, T. V., Sujith, A., Journal of Materials Science, **2017**, 52, 5708– 5725.
[4]Saf, A.O., Selcuk University Natural Sciences, **2010,** Konya.

Academic Partners

SAKARYA UNIVERSITY

SAKARYA UYGULAMALI BİLİMLER ÜNİVERSİTESİ 2018

KAFKAS ÜNİVERSİTESİ

IĞDIR ÜNİVERSİTESİ 2008

ADNSU AZƏRBAYCAN DÖVLƏT NEFT VƏ SƏNAYE UNİVERSİTETİ

Media Partners

LabMedya® CHEMLIFE ACS IraqChapter

Organization Partners

akpa

Global ACADEMIC PLATFORM